Genomic characterization of murine monocytes reveals C/EBPβ transcription factor dependence of Ly6C(-) cells

Mildner, A., Schönheit, J., Giladi, A., David, E., Lara-Astiaso, D., Lorenzo-Vivas, E., Paul, F., Chappell-Maor, L., Priller, J., Leutz, A., Amit, I., Jung, S.

This is the final version of the accepted manuscript. The original article has been published in final edited form in:

Immunity
2017 MAY 16 ; 46(5): 849-862
2017 MAY 16 (first published online)
doi: 10.1016/j.immuni.2017.04.018

Publisher: Cell Press / Elsevier

Genomic characterization of murine monocytes reveals C/EBPβ transcription factor dependence of Ly6C$^-$ cells

Alexander Mildner[1,4,†], Jörg Schönheit[2,4], Amir Giladi[1], Eyal David[1], David Lara-Astiaso[1], Erika Lorenzo-Vivas[1], Franziska Paul[1], Louise Chappell-Maor[1], Josef Priller[3], Achim Leutz[2], Ido Amit[1,†] and Steffen Jung[1,†] *

[1]Department of Immunology, Weizmann Institute of Science, Rehovot, Israel.
[2]Max Delbrück Center for Molecular Medicine, Berlin, Germany
[3]Department of Neuropsychiatry and Laboratory of Molecular Psychiatry, Charité Universitätsmedizin Berlin, Berlin, Germany

[4] authors contributed equally

* Lead contact : s.jung@weizmann.ac.il (S.J.)

[†] Corresponding author e-mails:

alexander.mildner@mdc-berlin.de (A.M.)
ido.amit@weizmann.ac.il (I.A.)
s.jung@weizmann.ac.il (S.J.)

SUMMARY

Monocytes are circulating, short-lived mononuclear phagocytes, which in mice and man comprise two main subpopulations. Murine Ly6C$^+$ monocytes display developmental plasticity and are recruited to complement tissue-resident macrophages and dendritic cells on demand. Murine vascular Ly6C$^-$ monocytes patrol the endothelium, act as scavengers and support vessel wall repair. Here we characterized population and single cell transcriptomes, as well as enhancer and promoter landscapes of the murine monocyte compartment. Single cell RNA-seq and transplantation experiments confirmed homeostatic default differentiation of Ly6C$^+$ into Ly6C$^-$ monocytes. The main two subsets were homogenous, but linked by a more heterogeneous differentiation intermediate. We show that intravascular monocyte differentiation occurred through *de novo* enhancer establishment and activation of pre-established (poised) enhancers. Generation of Ly6C$^-$ monocytes involved induction of the transcription factor C/EBPβ and C/EBPβ-deficient mice lacked Ly6C$^-$ monocytes. Mechanistically, C/EBPβ bound the *Nr4a1* promoter and controlled expression of this established monocyte survival factor.

147 words

INTRODUCTION

Monocytes are circulating, short-lived cells that are, together with tissue resident macrophages and dendritic cells (DC), classified as mononuclear phagocytes (Ginhoux and Jung, 2014). Adult steady state monopoiesis occurs in bone marrow (BM), where monocytes arise in a developmental sequence from dedicated precursor cells. Specifically, monocyte-macrophage DC progenitors (MDP) (Fogg et al., 2006) give rise to common monocyte progenitors (cMoP) committed to monocyte generation (Hettinger et al., 2013). Two main $CD14^{+}CD16^{-}$ and $CD14^{int}CD16^{+}$ monocyte populations have been identified in human blood (Passlick et al., 1989). Corresponding subsets in mice are defined as $CX_3CR1^{int}CCR2^{+}CD62L^{+}CD43^{low}Ly6C^{hi}$ ($Ly6C^{+}$) and $CX_3CR1^{hi}CCR2^{-}CD62L^{-}CD43^{hi}Ly6C^{lo}$ ($Ly6C^{-}$) cells (Geissmann et al., 2003; Palframan et al., 2001; Sunderkötter et al., 2004).

$Ly6C^{+}$ monocytes arise in the BM, where they represent the majority of monocytes (~90%). Once in the blood, $Ly6C^{+}$ monocytes are characterized by a high degree of developmental plasticity. Specifically, these cells sense injury and extravasate into tissues, where their descendants have emerged as a highly plastic cellular system that complements the classical tissue-resident mononuclear phagocyte populations, i.e. macrophages and DC (Mildner et al., 2013). Also during homeostasis, $Ly6C^{+}$ monocytes contribute to macrophage compartments of selected tissues (Varol et al., 2007; Molawi et al., 2014; Bain et al., 2016; Kim et al., 2016). The latter is likely related to environmental or physiological challenges of these organs and can vary among genders and mouse strains. $Ly6C^{-}$ monocytes are considered to remain in the vasculature. A fraction of these cells patrols the vessel walls, acting as scavengers and orchestrating tissue repair (Auffray et al., 2007; Carlin et al., 2013).

Circulating $Ly6C^{+}$ monocytes give rise to $Ly6C^{-}$ monocytes, as shown for mice and primates by sequential BrdU incorporation of the subset (Sugimoto et al., 2015; Yona et al., 2013), re-population kinetics following depletion regimes (Sunderkötter et al., 2004), and direct adoptive transfer of $Ly6C^{+}$ monocytes (Varol et al., 2007; Yona et al., 2013). Furthermore, following monocyte precursor engraftment, $Ly6C^{-}$ cells arise with delay compared to $Ly6C^{+}$ monocytes (Varol et al., 2007; Hettinger et al., 2013).

Development of both blood monocyte subsets depends on the 'pioneer' or lineage determining transcription factor PU.1 (encoded by *Spi1*; Scott et al., 1994). Mutations

of *Ccr2* (Serbina and Pamer, 2006), *Irf8* (Kurotaki et al., 2013) and *Klf4* (Alder et al., 2008; Feinberg et al., 2007) preferentially affect Ly6C$^+$ monocytes, while *Nr4a1* (Nur77) deficiency affects Ly6C$^-$ monocytes (Hanna et al., 2011). However, fate mapping experiments have shown that absence of Ly6C$^+$ monocytes can trigger a compensatory half-life extension of Ly6C$^-$ cells, and thereby mask the impairment of the Ly6C$^-$ compartment in mutants (Yona et al., 2013). Thus, deficiencies, including Irf8, Klf4 and CCR2, generally affect both monocyte subsets (Alder et al., 2008; Kurotaki et al., 2013; Yona et al., 2013). Likewise, also Nr4a1-deficient Ly6C$^+$ monocytes fail to compete with their wild type counterpart in mixed BM chimeric mice (Hanna et al., 2011).

Here we have systematically characterized the murine circulating monocyte subsets, including population-level and massively parallel single cell RNA sequencing (MARS-seq (Jaitin et al., 2014)), a global analysis of accessible chromatin regions (ATAC-Seq) and indexed chromatin immuno-precipitation (iChIP) to define epigenetic landscapes. We show that steady state differentiation of Ly6C$^+$ monocytes into Ly6C$^-$ cells ensued rapid transcriptomic changes accompanied by prevalent *de novo* gain of enhancer activity with only minor promoter changes. Including data from grafted Ly6C$^+$ monocytes, our results support and extend previous reports showing developmental progression from Ly6C$^+$ monocytes to Ly6C$^-$ cells. Mechanistically, we identified the induction of CCAAT-enhancer-binding protein beta (C/EBPβ) as part of the Ly6C$^-$ differentiation program, activating the monocyte survival factor Nr4a1, and show that C/EBPβ-deficiency impaired the generation of circulating Ly6C$^-$ monocytes.

RESULTS

Molecular characterization of murine monocytes and their progenitors. To map molecular determinants guiding monocyte development (**Fig. 1A**), we isolated MDP, cMoP, BM Ly6C$^+$ and Ly6C$^-$ monocytes, as well as the three phenotypically distinct Ly6C$^+$, Ly6C^{int} and Ly6C$^-$ blood monocyte populations from adult C57BL/6 mice (**Fig. 1B**) and performed a transcriptome analysis.

Comparative analysis of the populations revealed disparate regulation of 6064 genes (> two-fold differences in any pairwise comparison among a total of 15733 genes; **Fig. 1C, D** and **Fig. S1A**). A cluster defined by MDP (cluster I) was characterized by genes associated with a progenitor phenotype, including *Hoxa7*,

Cd34 and *Flt3* (**Fig. 1C, D**). Cluster II comprised genes co-expressed by MDP and cMoP, including *Kit, S1pr3*, *Myc* and *Myb* (**Fig. 1C, D**). Genes, such as *Cdk2*, *Cdk4* and members of the *Mcm* gene family indicated overrepresentation of the cell cycle pathway ($p = 3.5e^{-18}$, **Fig. S1B**). An even stronger enrichment of cell cycle genes was found in cluster III ($p = 1.6e^{-57}$, **Fig. S1B**) defined by high expression in cMoP and BM Ly6C$^+$ monocytes, indicating that at least a fraction of BM Ly6C$^+$ monocytes retained proliferative capacity, as reported earlier (Hettinger et al., 2013). Also classical Ly6C$^+$ monocyte genes like *Ly6c2* and *Sell* (CD62L) belonged to this cluster. Genes shared by Ly6C$^+$ monocytes in BM and blood were represented in cluster IV (694 genes), enriched for genes involved in response to viruses ($p = 2.7e^{-5}$, **Fig. S1B**) and comprising *Ccr2*, *Mmp8* and *Lgals3,* as well as the transcription factors *Cebpa*, *Fos* and *Cebpd* (**Fig. 1D**, **Fig. S1B**). Genes that showed a gradual increase of expression from Ly6C$^+$ to Ly6C$^-$ monocytes (including BM Ly6C$^-$ cells), formed cluster V, comprising *Cebpb*, *Klf2* and *Itgal* and genes involved in inflammatory pathways (**Fig. S1B**). Cluster VI included genes strongly up-regulated from Ly6C$^+$ to Ly6C$^-$ monocytes, such as *Pparg*, *Itgax* (CD11c) and *Nr4a1*. Therefore, *Cebpb* transcripts were already detectable in Ly6C$^+$ BM monocytes, whereas *Nr4a1* expression was induced in Ly6C$^+$ blood monocytes and increased in Ly6C$^-$ cells (**Fig. 1D**). Notably and supporting the notion that Ly6C$^-$ monocytes represent intra-vascular macrophages (Ginhoux and Jung, 2014), cluster VI also comprised genes characteristic of tissue resident macrophages, such as *Apoe* and *Cd36.*

Murine blood harbours, in addition to Ly6C$^+$ and Ly6C$^-$ populations, monocytes that display intermediate Ly6C and were interpreted as monocyte differentiation intermediates. The population-based analysis did not reveal a specific gene module unique to Ly6C^{int} monocytes; rather, these cells displayed an intermediate profile, sharing signatures with both Ly6C$^+$ and Ly6C$^-$ monocytes (**Fig. 1D**). Similar results were obtained with an independent data set, even though some differences between the experiments were evident, indicating the sensitivity of monocytes towards small environmental differences (**Fig. S2**).

Transferred BM Ly6C$^+$ monocytes adopt a transcriptional profile comparable to Ly6C$^-$ monocytes. The substantial expression changes between Ly6C$^+$ and Ly6C$^-$ monocytes suggested that linear progression of these cells (Sunderkötter et al., 2004; Varol et al., 2007; Yona et al., 2013) was driven by transcriptomic changes.

Transferred Ly6C$^+$ monocytes isolated from BM or spleen lose Ly6C expression and gain CX_3CR1, rendering them phenotypically indistinguishable from Ly6C$^-$ monocytes (Varol et al., 2007; Yona et al., 2013); however the molecular relationship of grafted monocytes and their derivatives to host monocyte populations had not been investigated.

To probe whether converted monocytes reflected the molecular changes seen in endogenous Ly6C$^-$ monocytes, we isolated CD117$^-$ CD11b$^+$ CD115$^+$ Ly6C$^+$ BM monocytes from CD45.1 congenic mice and transferred them into the bloodstream of CD45.2 WT animals (**Fig. 2A**). Cells were retrieved from recipient blood 24h, 36h and 48h after transfer, sorted based on their CD45.1, CD11b and CD115 expression and subjected to comprehensive transcriptional analysis (n=2 per time point, **Fig. 2B**). During this time, transferred monocytes gradually lost the Ly6C surface marker (**Fig. 2B**). Host Ly6C$^+$, Ly6C^{int} and Ly6C$^-$ blood monocyte populations were isolated alongside to control for potential injection-related side effects. In parallel, graft-derived cells were also retrieved from recipient spleens (**Fig. S3**).

Transcriptional profiling of monocyte samples revealed many genes to be differentially regulated in any pairwise comparison (1677 genes, **Fig. 2C**, **Fig. S4A**). We identified a cluster of genes specific for the Ly6C$^+$ BM monocyte graft (cluster I) (**Fig. 2C, D**). Importantly, genes of the 'Ly6C$^+$ monocyte gene signature' (including *Ccr2*, *Lyz2*, *Sell* and *Irf4*) were all down-regulated upon transfer, independently of the time point of retrieval (cluster II, III). Of note, Ly6C protein abundance persisted despite *Ly6c2* mRNA reduction in transferred cells 24h after transfer (**Fig. 2B,D**). Cluster V and VI on the other hand, comprised genes gradually up-regulated in transferred cells and shared with host Ly6C$^-$ monocytes. This included members of the 'Ly6C$^-$ gene signature', such as *Cx3cr1*, *Itgax*, *Bcl2, Pparg*, *Cd36*, as well as *Cebpb* and *Nr4a1*. Also genes associated with MHCII expression, such as *Cd74, H2-ab1* and *H2-eb1* were part of this cluster and higher expressed in cells re-isolated 24h after transfer compared to other time points. *Cd209a* was however absent from transferred cells (**Fig. 2D**). Genes highly expressed in Ly6C$^-$ host monocytes, but less prominent in grafted cells retrieved at 48h, grouped in cluster VII. Clusters IV and VIII comprised genes up-regulated shortly after monocyte transfer, which may be related to the *ex vivo* manipulation of the monocytes and transfer-associated stress.

To evaluate the relationship between grafted monocytes and their host counterparts, we compared expression of the 48h time point (without BM-specific

genes; cluster II-VIII) to the transcriptomes of host Ly6C$^+$, Ly6C^{int} and Ly6C$^-$ cells, respectively (**Fig. 2E**). Global correlation of gene expression of the transferred cells versus Ly6C$^+$ host cells was only moderate (r =0.51), while the correlation to Ly6C^{int} (r = 0.81) and Ly6C$^-$ (r = 0.85) host monocytes was higher (**Fig. 2E**), demonstrating their conversion. In contrast, the earlier 24h time point showed a higher correlation towards the Ly6C^{int} than Ly6C$^-$ monocyte phenotype (r = 0.79 vs. r = 0.69; **Fig. S4B**)

Collectively, our data demonstrate that as a population, 24h after transfer grafted Ly6C$^+$ monocytes in blood and spleen adopt a molecular signature that overlaps with Ly6C^{int} host cells and shifts 48h after transfer towards a Ly6C$^-$ monocyte profile.

Single cell RNA-Seq analysis reveals homogeneity of Ly6C$^+$ and Ly6C$^-$, but heterogeneity of Ly6C^{int} blood monocytes.

The transcriptional profiles described above were obtained from populations of sorted cells according to a limited number of canonical markers and bulk gene expression signatures may represent heterogeneous subsets with various dynamics (Paul et al., 2015). Although engrafted Ly6C$^+$ monocytes can acquire a phenotype and expression signature similar to Ly6C$^-$ host monocytes, remaining differences could indicate that Ly6C$^-$ monocytes represent a heterogeneous population of potentially distinct origins. To test this possibility, we performed MARS-seq (Jaitin et al., 2014; Paul et al., 2015) of Lin$^-$ CD11b$^+$ CD115$^+$ monocytes (1,098 cells) isolated from blood of adult C57BL/6 mice. For better resolution of intermediate monocytes we complemented this analysis with additional 365 Lin$^-$ CD11b$^+$ CD115$^+$ Ly6C^{int} monocytes (**Fig. S5A-C**).

Using indexed flow cytometry sorting followed by MARS-seq, we could relate expression profiles of individual cells to respective mean fluorescence intensities (MFI) of Ly6C and CD62L. *De novo* clustering analysis separated cells into 4 transcriptionally distinct subgroups, corresponding to Ly6C$^+$ and Ly6C$^-$ groups and two intermediate states (**Fig. 3A**, **Suppl. Tab. 1**). Expression analysis identified 477 differentially expressed genes (q < 1e-3, chi-square test), revealing heterogeneity within Ly6C^{int} monocytes. Cluster I corresponded to 224 cells with high Ly6C and CD62L MFI (**Fig. 3B**). Cluster II (148 cells) and cluster III (271 cells) comprised monocytes with intermediate surface Ly6C and CD62L expression. Cluster IV (820 cells) included cells with low Ly6C and low CD62L MFI. In line, the Lin$^-$ CD11b$^+$

CD115^{+} Ly6C^{int} monocyte subset was enriched for cells from clusters II and III (**Fig S5C**).

Focussing on gene expression, we could relate the gene program of Ly6C^{+} monocytes (including *Lyz1-2*, *Ccr2*, *Ly6c2*, *Mpeg1*, *Sell* and *Irf8*) to cluster I cells (**Fig. 3C**, **Fig. S5D**). Monocytes within cluster II, characterized by intermediate surface display of Ly6C and CD62L, showed specific expression of MHCII-related genes (*Cd74*, *H2-aa, Ciita*) and expressed *Ccr2*, as well as *Cd209a* (**Fig. S5E**). While our data closely link these cells to the Ly6C^{int} subset, they might be related to a recently reported monocyte subset biased to generate DC-like cells (Menezes et al., 2016). Surface MHCII expression by 50% of the Ly6C^{int} monocytes was further validated by flow cytometry analysis (**Fig. S5F**). Cluster III monocytes did not display a specific expression signature, but showed intermediate expression of *Cebpb*, *Nr4a1*, *Ccr2,* as well as MHCII-related genes. The 'Ly6C^{-} gene program', which included *Nr4a1*, *Cebpb*, *Cd36*, *Pparg*, *Itgax* and *Itgal*, was most evident in cluster IV monocytes (**Fig. 3C**).

To illustrate developmental relationship between the monocytes, we next used diffusion maps to project each single cell to a location in two-dimensional space (Haghverdi et al., 2015). All four clusters were separated territorially in the projected map (**Fig. 3D-E**). To further visualize expression patterns across the single cell data, we overlaid gene expression on the dimensionality reduction space. *Sell* and *Ly6c2* were found restricted to Ly6C^{+} monocytes in cluster I, while *Lyz2* and *Ccr2* expression was also shared by cluster II cells (**Fig. 3F**). Cluster II also specifically expressed *Cd209a*, MHCII-related genes, such as *H2-aa*, while *Cd36* was absent. Cluster III represented an intermediate subset that linked cluster I with cluster IV, i.e. Ly6C^{+} and Ly6C^{-} monocytes, characterized by induction of *Itgal*, *Cebpb* and *Cd36* expression. Expression of these genes peaked in cluster IV, and was accompanied by *Nr4a1* expression (**Fig. 3F**).

To investigate whether cluster II and III monocytes represent ontogenetically separate populations or related developmental stages, we analysed MARS-seq data of Lin^{-} CD11b^{+} CD115^{+} blood monocytes derived from *Cx$_3$cr1*^{cre}:*R26-YFP* animals. Due to the time-dependent probability of Cre-mediated genome editing of the *R26*-YFP locus of each individual cell, only few Ly6C^{+} monocytes express YFP in these mice, while all Ly6C^{-} monocytes are YFP^{+} (Yona et al., 2013). YFP expression can hence serve as a temporal indication of monocyte lifespan. Projecting these newly

sorted cells on our clusters (**Fig. 3A, Figs. S5G-H**), we identified the four clusters in *Cx3cr1*^{cre}:*R26-YFP* monocytes and related them to their YFP expression. In line, only 5,7% of the Ly6C$^+$ monocytes expressed YFP, whereas almost all (93,7%) of the Ly6C$^-$ were YFP positive (**Fig. 3G**). In contrast, half of the cells in clusters II and III expressed YFP (44,4% and 42,9% respectively), indicating that both stages are intermediate to the short-lived Ly6C$^+$ cells and the longer-lived Ly6C$^-$ monocytes.

Collectively, single cell RNA-Seq analysis established that Ly6C$^+$ and Ly6C$^-$ monocytes represent in steady state homogeneous populations, but reveal a certain degree of heterogeneity in the Ly6C^{int} monocyte compartment.

Chromatin analysis reveals gain of enhancer activity in Ly6C$^-$ monocytes with only minor promoter changes. Steady state conversion of short-lived Ly6C$^+$ into Ly6C$^-$ blood monocytes provides a unique model to study contributions of epigenetic changes in a rapid, physiologically relevant differentiation process. To investigate the epigenetic landscapes of murine Ly6C$^+$, Ly6C^{int} and Ly6C$^-$ blood monocytes, we profiled four histone modifications by indexing-first chromatin IP (iChiP) (H3K4me1, H3K4me2, H3K4me3, and H3K27ac; (Lara-Astiaso et al., 2014)) and performed an chromatin accessibility assay (transposase-accessible chromatin; ATAC-seq) (Buenrostro et al., 2013).

Histone modifications inform on the activity state of cis-acting genomic regulatory elements. Specifically, promoters are identified according to proximity to transcription start sites (TSS) and tri-methylation of lysine 4 on the histone H3 N-terminal tail (H3K4me3), while enhancers are defined by their distance from the TSS (>1kb) and enrichment of H3K4me1 and H3K4me2 marks (Heintzman et al., 2007). Enhancers can be further classified into 'poised' (H3K4me1$^+$) and active (H3K4me1$^+$, H3K27ac$^+$) (Creyghton et al., 2010).

Analysis of total H3K4me3 peaks (peak center <1kb from TSS) in the main monocyte subsets identified 9,635 promoters, 35 of which were differently used between Ly6C$^+$ and Ly6C$^-$ monocytes (**Fig. 4A**). This represents 0.36% differentially regulated H3K4me3 marks, whereas transcriptonal changes among the monocytes reached 8.4% (**Fig. 4B**). Of the altered H3K4me3-characterized promoters, seven showed loss during Ly6C$^+$ to Ly6C$^-$ differentiation, including *Sell*, *Clec5* and *Ly6c2* (**Fig. 4A,C**). 19 promoters were established *de novo* in Ly6C$^-$ monocytes, including *Bcl2a1b*, *Pparg*, *Cd36* and *Il1b*, while 8 promoters displayed an increased H3K4me3

signal in Ly6C$^-$ monocytes (**Fig. 4A,C**; **Suppl. Tab. 2**).

Analysis of distal H3K4me2 marks in the monocyte populations identified a total of 19,975 enhancers, 654 (3.3%) of which presented dynamic behavior. During the Ly6C$^+$ to Ly6C$^-$ differentiation, 35 enhancers lost marks (28 genes, e.g. *Ly6c2*, *Ccr1*) and 120 enhancers decreased their H3K4me2 signal (94 genes, e.g. *Ccr2*, *Sell*) this included one of the *Nr4a1* enhancers (**Fig. 4C**). Differentiation of Ly6C$^+$ to Ly6C$^-$ monocytes involved *de novo* mark acquisition of 181 enhancers, located in the vicinity of 129 genes, such as *Bcl2a1b*, *Klf4*, *Cd300e* and *Pparg;* additionally, 318 enhancers (211 genes, e.g. *Mir146*, *Sell*, *Nr4a1*, *Cd36*) increased their H3K4me2 signal during the Ly6C$^+$ to Ly6C$^-$ monocyte conversion (**Fig. 4A,C; Suppl. Tab. 2**). To confirm these results we characterized the distal H3K4me1$^+$ signal during the Ly6C$^+$ to Ly6C$^-$ conversion. H3K4me1 signal dynamics in enhancers followed a pattern similar to H3K4me2 (**Fig. 4A** and **Fig. S6B**), corroborating that Ly6C$^+$ to Ly6C$^-$ monocyte conversion involves *de novo* enhancer generation, rather than enhancer decommission, i.e. me1 and me2 de-methylation.

Finally, prominent changes were evident in histone acetylation, with 77 regions (60 genes) displaying reduced H3K27ac modification and 563 regions (313 genes) gaining acetylation during monocyte differentiation. This was consistent with the high number of *de novo* enhancers generated during the conversion.

Importantly, Ly6C^{int} monocytes were characterized by an overlapping phenotype and shared histone modification patterns with Ly6C$^+$ as well as Ly6C$^-$ monocytes, but lacked unique regulatory elements (**Fig. 4D**). Collectively, this revealed a specific and prevalent gain of enhancer activity in Ly6C$^-$ monocytes with only minor H3K4me3-marked promoter changes.

To define open chromatin regions and identify transcription factor binding motifs enriched for the specific monocyte populations, we applied ATAC-seq (Buenrostro et al., 2013) to circulating Ly6C$^+$, Ly6C^{int} and Ly6C$^-$ cells. Correlated replicates (**Fig. S6A**) allowed detection of 40,572 total accessible regions in all monocytes populations. Classical monocyte genes, such as *Cx3cr1*, *Nr4a1* and *Itgax*, showed an highly overlapping open chromatin pattern in all 3 populations, even though small subset-specific peak changes were evident - for instance in the *Nr4a1* and *Itgax* loci (**Fig. S6C**). Global quantification of differential ATAC peaks between Ly6C$^+$ and Ly6C$^-$ monocytes revealed 423 peaks (corresponding to 350 genes) that displayed a >2 fold enrichment in Ly6C$^+$ monocytes and 866 peaks (corresponding to

692 genes) that were increased in Ly6C$^-$ monocytes (**Fig. 4E**).

To identify potential transcription factors responsible for transcriptome and epigenome regulation during monocyte conversion, we examined the ATAC data for enrichment for transcription factor binding motifs within the differential accessible regions (Lara-Astiaso et al., 2014; Lavin et al., 2014). We identified both known and previously unknown candidate regulators, including Spi1 (Pu.1), Fosl2, Cebp and SpiC motifs enriched in Ly6C$^+$ monocytes and Nr4a1, Spi1, Cebp, Runx2 and Klf motifs enriched in Ly6C$^-$ monocytes (**Fig. 4F**).

We next compared the predicted motif enrichment in monocyte subsets with the transcription factor expression in these cells (**Fig. 4G**, **Fig. S6D**). *Spi1*, *Klf2*, *Klf4* and *Nr4a1* were prominently expressed in monocytes and increased with acquisition of the Ly6C$^-$ phenotype, confirming the requirement of these transcription factors for monocyte differentiation (Feinberg et al., 2007; Hanna et al., 2011; Scott et al., 1994). Notably, RNA-Seq analysis further revealed distinction within certain transcription factor families, such as the one comprising various members of the C/EBP family, which bind similar motifs and are therefore not resolved by chromatin footprint analysis. Within the C/EBP family, *Cebpb* was the most prominently expressed gene, correlating well with the predicted transcription factor motif analysis. Generally, monocyte conversion was associated with a shift from C/EBPα and δ to C/EBPβ prevalence (**Fig. 4G**).

Ly6C$^-$ monocytes are dependent on the transcription factor C/EBPβ.

Monocyte conversion was associated with prominent alterations within the C/EBP transcription factor family (**Fig. 4G**). Specifically, up-regulation of *Cebpb* in Ly6C$^-$ monocytes compared to Ly6C$^+$ cells, as well as after monocyte transfer suggested a role of C/EBPβ in late monocyte development (**Fig. 1C** and **Fig. 2D**). Indeed, monocytes were reported to be affected in C/EBPβ-deficient animals (Tamura et al., 2015), although it had not been addressed whether the effect was cell-intrinsic or restricted to a specific subset.

Analysis of peripheral blood of C/EBPβ-deficient mice and littermate controls revealed that Ly6C$^+$ monocytes were present in comparable frequency in both mouse strains, Ly6C^{int} monocytes showed a 50% reduction but Ly6C$^-$ blood monocytes were absent (**Fig. 5A**). Also BM Ly6C$^-$ monocytes were strongly reduced, while monocytic precursors, such as MDP, cMOP or BM Ly6C$^+$ monocytes were present at similar

frequencies in mutants and controls (**Fig. 5B**). To investigate, if the monocyte impairment of *Cebpb*$^{-/-}$ mice resulted from a cell-intrinsic defect, we performed a competitive repopulation assay, in which *Cebpb*$^{-/-}$ BM was mixed 1:1 with WT littermate BM and transplanted into lethally irradiated WT recipients. Analysis of the resulting chimeras 8 weeks after engraftment revealed that both genotypes contributed equally to MDP and cMoP (**Fig. 5C**). C/EBPβ-deficient BM cells had a disadvantage in generating Ly6C^{+} and Ly6C^{int} monocytes in BM and blood. Moreover, Ly6C^{-} monocytes were almost entirely derived from WT BM cells with hardly any C/EBPβ-deficient Ly6C^{-} monocytes detectable (ratio 95 +/- 33; **Fig. 5C**). These data establish the direct cell-intrinsic requirement of C/EBPβ for the generation or survival of Ly6C^{-} monocytes.

Encoded by an intron-less gene, C/EBPβ is expressed in distinct isoforms with different biological functions (Smink et al., 2009). A short, N-terminally truncated protein, the liver-enriched transcriptional inhibitory protein (LIP), lacks the transactivation domain and acts mainly as a dominant-negative C/EBPβ isoform (Descombes and Schibler, 1991). As compared to a C/EBPβ WT control (CoKi; C/EBPβ cDNA inserted into the *cebpb* locus) (Wethmar et al., 2010), expression of the C/EBPβ LIP isoform (Bégay et al., 2015) failed to rescue the developmental defect of Ly6C^{-} monocytes observed in *Cebpb*$^{-/-}$ mice (**Fig. 5D**). Moreover, LIP animals displayed a strong reduction in all monocyte subsets (**Fig. 5D**). The dominant effect of this physiological C/EBP inhibitor corroborates the importance of C/EBP transcription factor for monocyte differentiation and the requirement for proper C/EBP isoform balance.

To further dissect the impairment of the Ly6C^{-} monocyte compartment by the C/EBPβ deficiency, we isolated monocytes of *Cebpb*$^{-/-}$ mice and control littermates and performed RNA-Seq on these samples (**Fig. 5E**). Clustering of differentially expressed genes revealed that the 'Ly6C^{-} monocyte gene signature' was down-regulated in C/EBPβ-deficient Ly6C^{int} cells indicating a developmental block of the 'Ly6C^{-} gene program' (**Fig. 5E**). Respective gene clusters (I, II) included *Cebpb*, *Nr4a1*, *Bcl2* and *Itgal* (**Fig. 5F**). The 'monocytic Ly6C^{+} gene signature' including *Ly6c2*, *Lyz2*, *Sell* and *Fos,* was present in C/EBPβ-deficient Ly6C^{+} monocytes (cluster III, IV) (**Fig. 5F**). We also identified genes specifically up-regulated in Ly6C^{+} and Ly6C^{int} *Cebpb*$^{-/-}$ monocytes compared to controls (cluster V, VI). These clusters comprised other members of the C/EBP family, such as *Cebpa* and *Cebpe*,

suggesting compensation for or loss of repression by C/EBPβ. Also genes belonging to the 'MHC gene family', such as *H2-aa*, *H2-eb1* and *Cd74*, were higher expressed in C/EBPβ-deficient Ly6C^{int} monocytes (cluster VI**, Fig. 5F**). Similarly, *Cd209a* was strongly enriched in these cells, while *Cd36* was absent, indicating that the alternative differentiation pathway of Ly6C^{+} monocytes towards *Cd209a*-expressing Ly6C^{int} cells is probably C/EBPβ-independent.

C/EBPβ interacts with the Nr4a1 promoter and induces its expression.
Impaired development of Ly6C^{-} monocytes in *Cebpb*$^{-/-}$ mice and the profound competitive disadvantage of mutant cells over C/EBPβ-proficient monocytes (**Fig. 5A, C**) phenocopied Nr4a1-deficient animals (Hanna et al., 2011). Nr4a1 gene expression was strongly decreased in Ly6C^{int} *Cebpb*$^{-/-}$ monocytes (to 30 %; **Fig. 5F**), suggesting that C/EBPβ is involved in *Nr4a1* regulation.

To identify C/EBPβ binding sites at the *Nr4a1* locus, we examined the C/EBPβ binding pattern of cultured monocyte-derived cells (Bornstein et al., 2014). Two open chromatin regions upstream of the first exon of the *Nr4a1* gene were found in all monocyte subsets (-50bp (blue symbol) and -850bp (purple symbol) from the TSS). Sequence analysis revealed that all regions harboured C/EBPβ binding motifs (**Fig. 6A**). In these cells, the -850bp site was occupied by C/EBPβ, whereas the -50bp site displayed only a weak signal (**Fig. 6A**). Notably, this imperfect site had been reported earlier to be involved in C/EBPβ-dependent *Nr4a1* expression in rat cells (El-Asmar et al., 2009). In addition, a -4kb distal enhancer element was occupied by C/EBPβ (white symbol; **Fig. 6A**). To probe for differential contributions of the elements, we cloned combinations of regulatory regions upstream to a firefly luciferase gene reporter and transfected *Cebpb*$^{-/-}$ MEF cells with the constructs (**Fig. 6B**). Following introduction of ectopic C/EBPβ, we measured relative luciferase expression normalized to renilla luciferase activity. C/EBPβ addition did not induce luciferase expression in *Cebpb*$^{-/-}$ MEF cells transfected with control, the -50bp region or the -4kb enhancer plasmids (**Fig. 6B**). In contrast, constructs that contained the -850kb site showed a C/EBPβ-dependent increase in luciferase activity. Of note, the -4kb enhancer element in combination with the -850bp site further increased expression, but also affected the background signal in the absence of exogenous C/EBPβ, indicating C/EBPβ-dependent and independent interaction of these two regulatory elements. Collectively, our data suggest a critical role of C/EBPβ in the

regulation of Nr4a1 expression during monocyte conversion.

DISCUSSION

Monocytes and their descendants have emerged as a highly plastic and dynamic cellular system ensuring injury detection, robust inflammatory responses and resolution. Monocytes entail two main subpopulations currently defined as $CD14^+CD16^-$ and $CD14^{dim}$ $CD16^+$ cells in humans, and $Ly6C^+$ and $Ly6C^-$ cells in mice (Geissmann et al., 2003; Passlick et al., 1989). $Ly6C^+$ monocytes are inflammatory cells with tissue infiltrating capacity, while $Ly6C^-$ cells seem to remain in the circulation and control vessel wall integrity (Auffray et al., 2007; Geissmann et al., 2003).

$Ly6C^+$ monocytes give rise to $Ly6C^-$ monocytes. 'Converted' $Ly6C^+$ monocytes could represent a minor fraction of $Ly6C^-$ monocytes, but single cell RNA-Seq profiling did not reveal heterogeneity within $Ly6C^+$ and especially $Ly6C^-$ monocyte populations under steady state conditions. We can however not absolutely exclude that heterogeneity exists, or might arise following challenges, such as reported after IFN-γ injection (Askenase et al., 2015), as we sequenced only a small fraction (~0.5%) of all circulating monocytes.

Single cell analysis highlighted heterogeneity in the $Ly6C^{int}$ compartment by revealing a transient up-regulation of MHCII genes especially in these cells, which was also evident in the ATAC and iChIP analysis. Recently, a $MHCII^+$ cell population within the $Ly6C^+$ monocyte compartment was identified and proposed to give preferential rise to monocyte-derived DC (Menezes et al., 2016). Like our MHCII-expressing $Ly6C^{int}$ monocytes, these cells expressed the C-type lectin receptor CD209 (DC-SIGN). Transferred monocytes did not show any expression of *Cd209a* or MHCII-related genes after 48h, which could imply a direct conversion from $Ly6C^+$ towards $Ly6C^-$ monocytes without a $Cd209a^+$ intermediate stage. Notably, $Cd209a^+$ monocytes were also present in C/EBPβ-deficient mice and these cells could hence arise in the BM (Menezes et al., 2016). Our fate mapping approach suggests that $Ly6C^{int}$ *Cd209a*-expressing cells are short-lived and likely descendants of BM $Ly6C^+$ monocytes. Also human $CD14^+CD16^+$ double positive monocytes are characterized by higher MHCII expression (Gren et al., 2015; Schmidl et al., 2014; Zawada et al., 2011) and some human $CD14^+CD16^+$ monocytes may possibly represent equivalents of murine $MHCII^+$ $Ly6C^{int}$ monocytes.

Mechanistically, our findings suggest that C/EBPβ binds to promoter and enhancer regions of *Nr4a1* in monocyte-derived cells and activates *Nr4a1* expression. Nr4a1 has been previously shown to be obligatory for Ly6C$^-$ monocyte development (Hanna et al., 2011) Moreover, the same group showed recently that the second *Nr4a1* enhancer (E2) was crucial for Ly6C$^-$ monocyte development in a Klf2-dependent manner (Thomas et al., 2017). The authors subsequently focused on the control of *Nr4a1* expression by the E2 fragment and reported that it was independent of C/EBPβ, but under Klf2 control. We confirm these results, but show in addition that C/EBPβ binds to both enhancers (E1, E2) and thereby regulates expression of *Nr4a1*. The exact hierarchy of C/EBPβ and Nr4a1 induction remains unclear. We noted *Cebpb* expression in BM Ly6C$^+$ monocytes prior to *Nr4a1* induction, which appeared in blood Ly6C$^+$ and increased in Ly6C$^-$ monocytes. Furthermore, *Nr4a1* expression was reduced in Ly6C$^+$ and Ly6C^{int} monocytes isolated from C/EBPβ-deficient mice, indicating an upstream role of C/EBPβ. Likewise, Hanna et al. revealed a strong reduction of C/EBPβ expression in the remaining Ly6C$^-$ monocyte population isolated from Nr4a1-deficient mice (Hanna et al., 2011). Therefore it seems possible that both transcription factors are connected by a regulatory circuit. This is also supported by the fact that a small fraction of BM Ly6C$^-$ monocytes is still present in C/EBPβ-deficient mice – a observation similar to *Nr4a1*$^{-/-}$ animals (Carlin et al., 2013).

The phenotype of Nr4a1-deficient mice was attributed to a decreased survival of monocytes, accompanied by increased apoptosis in this cell lineage (Hanna et al., 2011). Similarly, *Cebpb*$^{-/-}$ monocytes show increased apoptosis (Tamura et al., 2015). However, C/EBPβ-deficient Ly6C^{int} monocytes lacked the Ly6C$^-$ monocyte gene signature, which was observed in C/EBPβ-proficient Ly6C^{int} cells, indicating a C/EBPβ function beyond a mere survival phenotype.

Collectively, our data indicate that Ly6C$^+$ monocytes represent an unstable cell population with a molecular and epigenetic default differentiation potential towards Ly6C$^-$ monocytes. However, even though Ly6C$^+$ cells seem to represent an *a priori* developmental stage, they are equipped with unique functional properties such as tissue infiltration and pro-inflammatory activity (Mildner et al., 2013), which cannot be acquired by Ly6C$^-$ monocytes (Varol et al., 2009). This raises the questions, whether the epigenetic landscape can change under inflammatory conditions to prevent the default differentiation into Ly6C$^-$ cells. It is possible that the observed shift in human

monocyte composition under pathological conditions towards increased abundance of $CD14^+CD16^+$ cells (reviewed in (Wong et al., 2012)) represents such a case. It will be critical to identify how plasticity is preserved in $Ly6C^+$ cells and how $Ly6C^+$ monocytes balance their developmental fate to either become circulating $Ly6C^-$ monocytes or to differentiate into monocyte-derived tissue macrophages.

CONTACT FOR REAGENT AND RESOURCE SHARING

Further information and requests for resources and reagents should be directed to and will be fulfilled by the Lead Contact, Steffen Jung (s.jung@weizmann.ac.il).

EXPERIMENTAL MODEL AND SUBJECT DETAILS

The following mouse strains have been used within this study: B6.Cg.129P2-C/EBPb tm1Pfj (C/EBPβ$^{-/-}$ (Sterneck et al., 1997)), B6.Cg.129P2-C/EBPtm3.2Acle (coki; (Wethmar et al., 2010)), B6.Cg.129P2-C/EBPtm1.2Acle (LIP; (Bégay et al., 2015)) and B6.Cg.129P2 (wt, littermate controls). These mice were kept on a mixed background. Female animals in an age between 6-12 weeks were used for analysis (related to Fig. 5 and Fig. S2). Female C57BL/6J (8 weeks) and CX$_3$CR1^{Cre} mice (Yona et al., 2012) crossed to Rosa-YFP mice (Srinivas et al., 2001; 16 weeks) were used for single cell sorting (related to Fig. 3 and Fig. S5). Female C57BL/6J (6-8 weeks) were used for bulk RNA-Seq (related to Fig. 1) and ChIP-Seq as well as ATAC-Seq (related to Fig. 4). For cell transfer experiments, BM monocytes from 8 weeks old female congenic B6.SJL-PtprcaPep3b/BoyJ (CD45.1) were injected into 8 weeks old female C57BL/6J mice (Harlan). For mixed BM chimeras, 8 weeks old female recipient animals (CD45.1/1) were lethally irradiated (950 rad) and reconstituted with female donor BM by i.v. injection of 10^6 BM cells isolated from C/EBPβ$^{-/-}$ (CD45.2/2), LIP (CD45.2/2) mice and mixed in a 1:1 ratio with littermate (CD45.1/2) BM cells. Mice were kept under Ciproxin (Bayer) antibiotics for 10 consecutive days and BM chimeras were analyzed 8 weeks after transfer. All mice were bred and maintained in specific pathogen-free (SPF) animal facilities at the MDC or the Weizmann Institute of Science. Animals were healthy and they were healthy and they were not involved in previous procedures. Experiments were approved by an Institutional Animal Care Committee (IACUC) in accordance to international guidelines.

METHOD DETAILS

Flow cytometry and cell sorting

Antibodies against CD11b (M1/70), CD11c (HL3), CD115 (AFS98), CD117 (2B8), Ly-6C (HK1.4), CD135 (A2F10), Ly6G (1A8), CD19 (6D5), CD3e (145-2c11), CD45.1 (A20), CD45.2 (1D4), B220 (RA3-6B2), CD62L (MEL-14), MHCII (IAb; AF6-102.1), TCRγδ (GL-3), Ter119, NK1.1 (PK136) from Biolegend or eBioscience were used.

For sequencing, monocytes were isolated by CD115 biotin antibodies followed by anti-biotin MACS without RBC lysis. Monocytes were identified as lineage negative (Ter119, B220, CD19, CD3, NK1.1, Ly6G, TCRγδ), CD11b^{+} and CD115^{+}. Samples were flow sorted either using AriaII, AriaIII or Aria-Fusion (BD Biosciences, BD Diva Software) cell sorter. Analysis was performed on Fortessa or LSRII (BD Biosciences, BD Diva Software) and analyzed with FlowJo software (Treestar).

Bulk RNA sequencing

RNA-Seq of populations was performed as described previously (Lavin et al., 2014). In brief, 10^3–10^5 cells from each population were sorted into 50µl of lysis/binding buffer (Life Technologies) and stored at -80°C. mRNA was captured with Dynabeads oligo(dT) (Life Technologies) according to manufacturer's guidelines. We used a derivation of MARS-seq (Jaitin et al., 2014). Briefly, RNA was reversed transcripted with MARS-Seq barcoded RT primer in a 10µl volume with the Affinity Script kit (Agilent). Reverse transcription was analyzed by qRT-PCR and samples with a similar CT were pooled (up to 8 samples per pool). Each pool was treated with Exonuclease I (NEB) for 30min 37°C and subsequently cleaned by 1.2X SPRI beads. Afterwards, the cDNA was converted to double-stranded DNA with a second strand synthesis kit (NEB) in a 20µl reaction, incubating for 2.5 h at 16℃. The product was purified with 1.4x volumes of SPRI beads, eluted in 8µl and in-vitro transcribed (with the beads) at 37°C overnight for linear amplification using the T7 High Yield RNA polymerase IVT kit (NEB). Following IVT, the DNA template was removed with Turbo DNase I (Ambion) 15 min at 37°C and the amplified RNA (aRNA) purified with 1.2x volumes of SPRI beads. The aRNA was fragmented by incubating 2.5min at 70°C in Zn2+ RNA fragmentation solution (Ambion) and purified with 2X SPRI beads. The aRNA (5µl) was preincubated 3 min at 70°C with 1µl of 100µM MARS seq ligation adapter; then, 14µl of a mix containing 9.5% DMSO, 1mM ATP, 20% PEG8000 and 1 U/µl T4 ligase (NEB) in 50 mM Tris HCl pH7.5, 10 mM MgCl2 and 1mM DTT was added. The reaction was incubated at 22°C for 2 h. After 1.5X SPRI cleanup, the ligated product was reverse transcribed using Affinity Script RT enzyme (Agilent; reaction mix contains Affinity Script RT buffer, 10 mM DTT, 4 mM dNTP, 2.5 U/µl RT enzyme) and a primer complementary to the ligated adapter. The reaction was incubated for 2min at 42°C, 45 min at 50°C and 5 min at 85°C. The cDNA was purified with 1.5X volumes of SPRI beads. The library was completed and amplified

through a nested PCR reaction with 0.5 µM of P5_Rd1 and P7_Rd2 primers and PCR ready mix (Kapa Biosystems). The amplified pooled library was purified with 0.7X volumes of SPRI beads to remove primer leftovers. Library concentration was measured with a Qubit fluorometer (Life Technologies) and mean molecule size was determined with a 2200 TapeStation instrument. RNA-Seq libraries were sequenced using Illumina NextSeq-500. Raw reads were mapped to the genome (NCBI37/mm9) using hisat (version 0.1.6). Only reads with unique mapping were considered for further analysis. Gene expression levels were calculated using the HOMER software package (analyzeRepeats.pl rna mm9 -d <tagDir> -count exons -condenseGenes -strand + -raw) (Heinz et al., 2010). Normalization and differential expression analysis was done using the DESeq2 R-package. Differential expressed genes were selected using a 2-fold change cutoff between at least two populations and adjusted pValue for multiple gene testing > 0.05. Gene expression matrix was clustered using k-means algorithm (matlab function kmeans) with correlation as the distance metric. The value of k was chosen by assessing the average silhouette (matlab function silhouette) (3) for a range of possible values (4-15).

Indexing-first chromatin IP (iChIP) sequencing

10^5 crosslinked cells were used for iChIP-seq, as described (Lara-Astiaso et al., 2014). Briefly, following crosslinking for 8 min in 1% formaldehyde and quenched for 5min in 0.125 M glycine, cells were FACS sorted, diluted in harvesting buffer (12mM Tris-HCl, 0.1X PBS, 6mM EDTA, 1.2X Protease Inhibitor (Roche)), pelleted by two rounds of centrifugation (15min, 3000g, low acceleration and brake) and frozen at -80°C. Cell aliquots (around 10µl) are thawed on ice and 2µl of 3% SDS is added to achieve a concentration of 0.5% SDS. Chromatin was fragmented by sonication at high intensity and cycles of 30” ON/30” OFF with the NGS Bioruptor Sonicator (Diagenode) for 40min. Cells were diluted 1:5 with sonication equilibration buffer (10mM Tris-HCl, 140mM NaCl, 0.1% sodium deoxycholate, 1% Tx-100, 1mM EDTA, 1X Protease Inhibitor) and sheared chromatin was immobilized on 15µl Dynabeads Protein G (ThermoFisher) with 1.3µg of anti-H3 antibody (ab1791, Abcam) for 20h on 4°C. The H3-bound beads were magnetized and washed 3 times with 150µl 10mM Tris-HCl, 1X Protease Inhibitors and resuspended in 20µl of the same buffer. Chromatin End Repair was performed by adding 30µl of a master mix: 25µl 2X ER mix (50mM Tris-HCl ph 7.5, 20mM MgCl2, 20mM DTT, 2mM ATP, 1mM dNTPs), 2µl

T4 PNK enzyme (10 U/µl NEB), and 2µl T4 polymerase (3 U/µl NEB) to each sample and incubated at 12°C for 25min, 25°C for 25min, and finally cooled to 4°C. After end repair, bead bound chromatin was washed once with 150µl of 10mM Tris-HCl + Protease Inhibitors and re-suspended in 40µl of the same buffer. Chromatin was A-tailed by adding 20µl master mix (17µl A-base add mix, 3µl Klenow (3'->5' exonuclease, 3 U/µl, NEB) to each well and incubated at 37°C for 30 min. Afterwards, bead bound chromatin was washed once with 150µl of 10mM Tris-HCl + Protease Inhibitors and resuspended in 19µl of the same buffer. Chromatin was indexed by adding 5µl of 0.75µM Y- shapped Indexed Adaptors (containing P5 and P7 sequences) to each well which were ligated to the chromatin's DNA ends by adding 34µl of AL master mix (29µl 2x Quick Ligation Buffer and 5 µl Quick DNA ligase (NEB)) to each well. Samples were mixed and incubated at 25°C for 40min in a thermal cycler. Bead bound indexed chromatin was washed once as described above in order to remove non-ligated adaptors. After wash, samples were removed from the magnet, beads were re-suspended in 12.5µl of 100mM DTT and incubated for 5min at room temperature. Then, 12.5µl of 2X Chromatin Release Buffer (500mM NaCl, 2% SDS, 2% Sodium Deoxycholate, 2X protease Inhibitors) was added, samples were mixed and incubated at 37°C for 30min. After the release incubation, magnetic beads were again thoroughly re-suspended and pooled together in groups of <10 samples resulting in a pool volume of 200-250µl. The pooled indexed chromatin samples were concentrated using a 50Kda cutoff Centricon (Amicon). Target antibody was added and incubated at 4°C for 3h, then 50µl with Protein G Magentic beads were added and IP was incubated for 1 more hour. For each ChIP, we used 1.5µg of anti-H3K4me1 (ab8895; Abcam) and 2.5µg of anti-H3K4me2 (ab32356; Abcam), anti-H3K4me3 (07-473; Millipore) and anti-H3K27ac (ab4729; Abcam). After incubation, ChIP Buffer was removed and samples were washed 5 times with cold RIPA (200ul per wash), twice with RIPA buffer supplemented with 500mM NaCl (200ul per wash), twice with LiCl buffer (10mM TE, 250mM LiCl, 0.5% NP-40, 0.5% DOC), once with TE (10Mm Tris-HCl pH 8.0, 1mM EDTA), and then eluted in 50µl of 0.5% SDS, 300mM NaCl, 5mM EDTA, 10mM Tris-HCl pH 8.0. The eluate was treated sequentially with 2µl of RNaseA (Roche, 11119915001) for 30 min at 37°C, 2.5µl of Proteinase K (NEB, P8102) for additional two hours at 37°C and 8 hours at 65°C to revert formaldehyde crosslinking. DNA was purified with SPRI beads (90µl, Agencourt AMPure XP beads, Beckman Coulter) according to

manufacture's protocol. The DNA was eluted in 23µl EB buffer (10mM Tris-HCl, pH 8.0) by pipette mixing 25 times. The library was completed and amplified through a PCR reaction with 0.5µM of PCR forward and PCR reverse primers and PCR ready mix (Kapa Biosystems). Following the amplification step, DNA concentration was measured, and equivalent amounts of barcoded ChIPed DNA from each sample were pooled together. After barcoding, pooled DNA was sequenced (HiSeq 1500, Illumina) to achieve a minimum of 10^7 aligned reads per sample.

ATAC sequencing

20,000 cells were used for ATACseq (Buenrostro et al., 2013) applying described changes (Lara-Astiaso et al., 2014). Briefly, nuclei were obtained by lysing the cells with cold lysis buffer (10mM Tris-HCl pH 7.4, 10mM $MgCl_2$, 0.1% Igepal CA-630) and nuclei were pelleted by centrifugation for 30min at 500g, 4°C using a swing rotor with low acceleration and brake settings. Supernatant was discarded and nuclei were re-suspended in 25µl reaction buffer containing 2µl of Tn5 transposase and 12.5µl of TD buffer (Nextera Sample preparation kit from Illumina). The reaction was incubated at 37°C for one hour. DNA was released from chromatin by adding 5µl of clean up buffer (900mM NaCl, 300mM EDTA), 2µl of 5% SDS and 2µl of Proteinase K (NEB) followed by a incubation for 30min at 40ºC. Tagmentated DNA was isolated using 2x SPRI beads and eluted in 21µl. For library amplification, two sequential 9-cycle PCR were performed in order to enrich small tagmentated DNA fragments. We used 2µl of indexing primers included in the Nextera Index kit and KAPA HiFi HotStart ready mix. After the first PCR, the libraries were selected for small fragments (less than 600 bp; 0.65X) using SPRI cleanup. Then a second PCR was performed with the same conditions in order to obtain the final library. DNA concentration was measured with a Qubit fluorometer (Life Technologies) and library sizes were determined using TapeStation (Agilent Technologies). Libraries where sequenced on a Hiseq 1500 for an average of 20 million reads per sample

Processing of ChIP-Seq and ATAC-Seq

Reads were aligned to the mouse reference genome (mm9, NCBI 37) using Bowtie2 aligner version 2.2.5 (Langmead et al., 2009) with default parameters. The Picard tool MarkDuplicates from the Broad Institute (http://broadinstitute.github.io/picard/) was used to remove PCR duplicates. To identify regions of enrichment (peaks) from

ChIP-seq (H3K4me1, H3K4me2, H3K4me3 and H3K27ac), we used the HOMER package makeTagDirectory followed by findPeaks command "-style histone". For ATACseq we used makeTagDirectory followed by findPeaks command "-style factor -size 300", respectively (Heinz et al., 2010). Union peaks file were generated for each of H3K4me1, H3K4me2, H3K4me3 and H3K27ac by combining and merging overlapping peaks in all samples.

Chromatin and Motif Analysis

All ChIP-seq peaks were binned to 1kb size. To create the table of samples, we used annotatePeaks.pl from HOMER package passing the binned peak file and option "-raw" and normalized to an equal number of reads in merged peaks. We consider promoters to be peak center < 1kb from TSS of nearest gene. H3K4me3 regions used are only near promotor areas, while binned the peaks of H3K4me1, H3K4me2 and H3K27ac used are all non-promotor areas. Noise was set at ~80% of all normalized value. The region intensity was given in log-base2 of the normalized density (log2(x+1)). Fold change bins were considered changing when delta between samples (log2(x+noise)) was > 1 (red line in Fig. 4A). Kmeans clustering was performed using MATLAB function kmeans with the distance metric set to ‘‘correlation". Motif Analysis was performed inside ATAC peaks and differential regions were used as input for the HOMER package motif finder algorithm findMotifGenome.pl (Heinz et al., 2010).

Single cell sequencing

MARS-seq reads were processed as previously described (Paul et al., 2015). Briefly, mRNA from cells sorted into MARS-seq capture plates was barcoded and converted into cDNA and pooled using an automated pipeline. The pooled sample was then linearly amplified by T7 in-vitro transcription and the resulting RNA was fragmented and converted into a sequencing-ready library by tagging the samples with pool barcodes and Illumina adapter sequences during ligation, followed by reverse transcription and PCR. Each pool of cells was tested for library quality and concentration as described earlier (Jaitin et al., 2014). All RNA-Seq libraries (pooled at equimolar concentration) were sequenced using an Illumina NextSeq 500. Mapping of reads was done using hisat (version 0.1.6) to mm9 genome. Reads with multiple mapping positions were excluded. Reads were associated with genes, if they

were mapped to an exon defined by a reference set obtained from Gencode. Exons of different genes that share genomic position on the same strand were considered as a single gene with concatenated gene symbol. Cells with less than 200 UMIs were discarded from the analysis. Genes with mean expression smaller than 0.005 UMIs/ cell or with above average expression and low coefficient of variance (< 1.2) were also discarded. In order to assess the heterogeneity of blood monocyte subtypes, we used a recently published multinomial mixture-model algorithm (Paul et al., 2015) (http://compgenomics.weizmann.ac.il/tanay/?page_id=649). A brief summary of the algorithm is described below and its detailed description can be found in our earlier publication (Paul et al., 2015). Low-level processing of MARS-Seq reads results in a matrix U with n rows and m columns, where rows represent genes and columns represent cells. Entry Uij contains the number of unique molecular identifiers (UMIs) from gene i that were found in cell j. The model assumes that each cell belongs to one of K cell types, and that each cell type defines a different distribution of transcripts within cells.

Our model assumes that cells are sampled uniformly from the population, and that each cell type dictates a multinomial distribution over the sample of sequenced RNA molecules. The model consists of three types of parameters:

□□□□ - The assignment of cell j to one of K cell types.

□□,□□□□ - the probability of observing gene i in cell j, assuming that j belongs to cell type □□□□.

□□□□ - a positive inflation factor accounting for batch effect on the expression of gene i (b^j is the batch of cell j).

A pseudo EM algorithm was used to infer the assignment of cells to types, gene probability within cell type, and magnitude of batch effect. The algorithm outline is as follows:

1. Initialize the model:

a. Estimate β (batch effect vector) from the gene expression in each batch.

b. Sample a first seed for the cell types at random by drawing uniformly from the list of cells.

2. Repeat a-d to generate the desired number of clusters:

a. Initialize a pre-seed model using the regularized transcripts of the seed cell.

b. Find the set of D cells with the highest likelihood to the pre-seed model. Using these cells, initialize a new set of parameters α and optimize the likelihood of the

selected cells given these parameters and given constant batch parameters. Optimization is done using non-linear optimization procedure (L-BFGS-B). Add the optimized parameters as a new component to the model.

c. Compute the log-likelihood of each cell to each of the current initialized types. Assign each cell to its corresponding maximum-likelihood cell type.
d. Sample a new seed cell at random by drawing from quantiles 0-0.05 of the maximum likelihoods obtained in c.

3. Given the current set of multinomial models, calculate the assignment for each cell (□□□□) by calculating the maximum assignment probability.
4. Given the current β and map parameters, use L-BFGS-B to find α (for each cell type) that maximizes the likelihood of the U matrix.
5. Given the current α and the map parameters, use L-BFGS-B to find β that maximizes the likelihood of the U matrix.
6. Return to step 2 and repeat until the likelihood function converges, or the maximum number of iterations is reached.

Since samples derive from different sorting schemes, clustering was performed with fixed β values. Dimensionality reduction was performed on log2-transformed normalized UMI matrix containing the 477 variable genes by using the diffusion map method (destiny package (Haghverdi et al., 2015)). Projection of genes on the 2D map shows normalized values, smoothed by proximity in 2D Euclidean space.

Luciferase reporter assay

$2x10^5$ C/EBPβ$^{-/-}$ MEF cells were seeded in triplicates in 12-well plates 12h prior transfection, 500ng Nr4a1 Firefly-luciferase reporter construct (in pGL4.10; Promega), 100ng C/EBPβ in a pcDNA3.1 background or empty pcDNA3.1 (Addgene) were co-transfected together with 10ng of a Renilla-luciferase pGL4.70 vector (Promega) using PEI. Luciferase expression was assed after 48h using a Berthold Luminometer (Centro LB 960). Firefly-luciferase expression was normalized to Renilla-luciferase activity to control for transfection efficiency. The data are representative of four independent experiments, results from one experiment are plotted as the mean ± SEM.

QUANTIFICATION AND STATISTICAL ANALYSIS

In all experiments, data are presented as mean ± STD if not stated otherwise. Statistical tests were selected based on appropriate assumptions with respect to data distribution and variance characteristics. Student's t test (two-tailed) was used for the statistical analysis of differences between two groups. Statistical analyses were done applying Students t-test for the calculation of the P-value. Statistical significance was defined as $P<0.05$. Sample sizes were chosen according to standard guidelines. Number of animals is indicate as 'n'. Of note, sizes of the tested animal groups were also dictated by availability of the transgenic strains and litter sizes, allowing littermate controls. Pre-established exclusion criteria are based on IACUC guidelines. As for in vitro experiments, samples were excluded from analysis only in case of clear technical problems. Animals of the same age, sex and genetic background were randomly assigned to treatment groups. The investigator was not blinded to the mouse group allocation. Tested samples were blindly assayed.

ACCESSION NUMBERS

The accession numbers for the RNA-, ChIP- and ATAC-seq datasets reported in this paper can be found at GEO: GSE95702.

SUPPLEMENTAL INFORMATION

Supplemental Information includes Supplemental Experimental Procedures and six figures and two tables and can be found with this article online at .....

AUTHOR CONTRIBUTIONS

A.M., I.A. and S.J. conceived the project and designed the experiments; A.M. and J.S., E. L.-V., D. L-A. and F.P. performed the experiments; A.M., E.D. and A.G. analyzed the data. A.L. and J.P. advised on experiments; A.M., I.A. and S.J. wrote the paper; I.A. and S.J. supervised the project.

ACKNOWLEDGEMENTS

We would like to thank all members of the Jung laboratory, as well as Simon Yona for helpful discussion. We further thank the staff of the Weizmann Animal facility and the members of the FACS facility for expert advice. Work in the Jung laboratory was supported by the Israeli Science Foundation (887/11), the European Research Council (AdvERC grant 340345), the BSF and the Deutsche

Forschungsgemeinschaft (CRC/TRR167 “NeuroMac” (for SJ, IA). A.M is a Heisenberg fellow supported by the DFG (MI1328). A.G. is supported by a Clore Scholarship. I.A. is supported by the European Research Council Consolidator Grant (ERC-COG) 724471-HemTree2.0; the Israel Science Foundation; the Ernest and Bonnie Beutler Research Program of Excellence in Genomic Medicine; the Helen and Martin Kimmel award for innovative investigation; a Minerva Stiftung research grant and the Israeli Ministry of Science, Technology, and Space.

FIGURE LEGENDS

Figure 1. Monocyte development is accompanied by transcriptome changes.

(A) Schematic of monocyte differentiation.

(B) Exemplary flow cytometry analysis of murine monocyte identification.

(C) Expression analysis of murine MDP, cMoP, BM Ly6C$^+$ as well as BM Ly6C$^-$ monocytes and the three circulating blood monocyte subsets Ly6C$^+$, Ly6C^{int} and Ly6C$^-$ by RNA-Seq. Analysis was restricted to genes, which showed a 2-fold difference in at least one cell population and sample. K-means clustering was set to n = 6. See also related **Fig. S1** for GO-enrichment and TF expression in monocyte subsets. 3-4 mice were used for this experiment. Similar results of an independent experiment can be found in **Fig. S2**.

(D) Examples of gene expression from the six identified clusters depicted in C. Shown are the mean sequence reads ± STD.

Figure 2. Transferred BM Ly6C$^+$ monocytes develop on the molecular level into Ly6C$^-$ monocytes.

(A) Schematic view of monocyte transfer experiment. CD45.1$^+$ Ly6C$^+$ BM monocytes were purified by flow cytometry sorting and 2x10^5 cells were injected into CD45.2 congenic mice. 24h, 36h and 48h hours after injection, the transferred CD45.1$^+$ CD11b$^+$ CD115$^+$ monocytes were re-isolated from the blood by flow cytometry sorting and analyzed by RNA-Seq. Ly6C$^+$, Ly6C^{int} and Ly6C$^-$ monocytes from the host mice were analyzed by RNA-Seq in parallel and served as control. Similar results were obtained for the spleen (**Fig. S3**).

(B) Histogram (left panel) and mean fluorescence intensity (MFI; right panel) of Ly6C expression on transferred monocytes 24h (red), 36h (grey) and 48h (blue) hours after injection. Note that Ly6C protein abundance dropped rapidly between 24h and 48h. Two recipients per time point were analyzed and the mean MFI ± STD are shown.

(C) Expression analysis of transferred monocytes before, 24h, 36h and 48h after injection as well as host Ly6C$^+$, Ly6C^{int} and Ly6C$^-$ monocyte subsets by RNA-Seq. Samples were analyzed in duplicates and analysis was restricted to genes, which showed a 2-fold difference in at least one cell population and sample. K-

means clustering was set to n = 8. Respective GO-enrichment can be found in **Fig. S4A**.

(D) Examples of expression levels from individual genes identified by the cluster analysis depicted in C. Shown are the mean sequence reads ± STD.

(E) Correlation analysis of the expression signature of monocytes isolated 48h after transfer against host Ly6C^{+}, Ly6C^{int} and Ly6C^{-} monocyte subsets. The 1472 differential expressed genes without the BM-specific cluster I shown in C were included (cluster II-VIII) and the average of the duplicates were used for calculation. Sequence reads are presented as log_2 values. See also related **Fig. S4B**.

Figure 3. Single cells sequencing of murine blood monocytes

(A) Top: Clustering of 1463 monocytes according to their gene expression profile. Four main clusters could be identified. Shown are on the X-axis cells and on the Y-axis genes. Shown are 359 differential expressed genes with >100 UMI count. See **Fig. S5A-F** for more details.

(B) MFI of Ly6C and CD62L expression based on indexed FACS analysis for the 1098 sequenced monocytes excluding the specifically sorted Ly6C^{int} cells (365 cells).

(C) Marker gene expression in each cluster.

(D) Diffusion map 2D projection of all sequenced single cells, coloured by their assignment to the four monocyte clusters identified in **Fig. 3A**.

(E) Black and white depiction of the localisation of the four clusters in the dimensionality reduction map.

(F) Overlay of individual gene expression on the reduction map.

(G) An additional set of 666 single cell monocytes were sequenced from *Cx$_3$cr1*^{Cre}:*R26-YFP* mice and assigned to the four clusters by their maximum likelihood. Through indexed flow cytometry sorting, each single cell could be related to their YFP expression, thereby identifying cluster II and cluster III cells as short-lived (BM) Ly6C+ monocyte-descendants. See also **Fig. S5G-H** for detailed analysis.

Figure 4. The epigenetic landscape of murine monocytes.

(A) Summary of histone modifications (H3K4me1, H3K4me2, H3K4me3 and

H3K27ac) in blood Ly6C$^+$ and Ly6C$^-$ monocytes. Data were acquired as duplicates for all monocyte populations (**Fig. S6A**) and the signal for each population was merged for comparative analysis. Data are represented as log_2.

(B) Summary of expression (RNA), methylation (H3K4me1, H3K4me2, H3K4me3 and H3K27ac) and open chromatin (ATAC) changes in Ly6C$^+$ and Ly6C$^-$ monocytes. Shown are the percentages of 2-fold changing gene peaks compared to all detected gene peaks.

(C) Examples of H3K4me2 (the first three rows), H3K4me3 (middle rows) and H3K27ac (lower three rows) in Ly6C$^+$ (dark red), Ly6C^{int} (red) and Ly6C$^-$ monocytes (orange). Corresponding H3K4me1 signal can be found in **Fig. S6B**. Blue areas indicate changing promoters and green areas changing enhancers.

(D) Heatmap of differential modified gene loci with at least 2-fold change in Ly6C$^+$, Ly6C^{int} or Ly6C$^-$ monocytes, respectively. Note the intermediate phenotype of Ly6C^{int} monocytes in sharing histone marks with either Ly6C$^+$ or Ly6C$^-$ monocytes.

(E) Analysis of all 40,572 detected ATAC peaks, from which 423 peaks showed an at least 50% higher read count in Ly6C$^+$ monocytes (dark red) and 886 peaks were enriched in Ly6C$^-$ monocytes (orange). Examples of IGV tracks can be found in **Fig. S6C**.

(F) Homer motif enrichment for TF binding sites in genes that are either more open in Ly6C$^+$ monocytes (423 genes; upper graph) or in Ly6C- monocytes (886 genes; lower graph). Shown are the p-values (in log_{10}) and the corresponding motifs.

(G) Gene expression of TF in Ly6C$^+$, Ly6C^{int} and Ly6C$^-$ monocytes that were identified by the motif enrichment in F. Shown are the mean sequence reads ± STD. More related genes can be found in **Fig. S6D**.

Figure 5. Ly6C$^-$ monocyte development depends on the expression of C/EBPβ.

(A) Flow cytometry analysis of blood monocytes isolated from C/EBPβ-deficient mice and littermate controls. Monocytes were identified as CD11b$^+$ and CD115$^+$ and separated according to Ly6C and CD11c expression. Two independent experiments were pooled. N = 6-8 mice. Each symbol represents one animal. Asterisk indicates statistical difference with $p < 0.05$ according to student's t-test.

(B) Frequency of BM monocyte populations and their precursors out of Lin^{neg} CD115$^+$ cells isolated from C/EBPβ-deficient mice and littermate controls. 4 animals per

group were used and each symbol represents one animal. Asterisk indicates statistical difference with $p < 0.05$ according to student's t-test.

(C) Mixed bone marrow chimera experiment in which C/EBPβ-deficient CD45.2 BM cells were mixed with CD45.1-2 littermate BM cells and injected into lethally irradiated CD45.1 recipients. Analysis of the indicated cell populations was performed 8 weeks after transfer and shown is the log_{10} ratio of CD45.1-2$^+$ cells to CD45.2$^+$ cells. 4 animals were used in this experiment and each symbol represents one recipient. The experiment was performed twice with similar results.

(D) Analysis of transgenic mice, which express in the wt C/EBPβ locus either the short, N-terminally truncated C/EBPβ version LIP or the wt full-length C/EBPβ construct (coki). Monocytes were identified as CD11b$^+$ CD115$^+$ and separated according to Ly6C and CD11c expression. 4-6 animals were analyzed and each symbol represents one animal. Asterisk indicates statistical difference with $p < 0.05$ according to Student's t-test.

(E) Gene expression analysis by RNA-Seq of C/EBPβ-deficient and littermate monocytes. Since Ly6C$^-$ monocyte were strongly reduced in C/EBPβ$^{-/-}$ mice, only Ly6C$^+$ and Ly6C^{int} monocytes were analyzed from this genotype. Samples were analyzed in duplicates and analysis was restricted to genes, which showed a >2-fold difference in at least one cell population and sample. K-means clustering was set to n = 6.

(F) Examples of gene expression in wt and C/EBPβ-deficient monocytes. Shown are the mean sequence reads ± STD. Note the strong up-regulation of MHCII-related genes in C/EBPβ-deficient Ly6C^{int} monocytes.

Figure 6. C/EBPβ binds to *Nr4a1* enhancer elements and induces *Nr4a1* expression

(A) Open chromatin structure of the first *Nr4a1* enhancer elements in Ly6C$^+$, Ly6C^{int} and Ly6C$^-$ blood monocytes (black IGV tracks) as well as *in vitro* monocyte-derived cells (grey IGV track; data was taken from (Bornstein et al., 2014)). ChIP analysis of C/EBPβ-bound chromatin regions in *in vitro* monocyte-derived cells (red IGV track; data was taken from (Bornstein et al., 2014)) shows the binding of C/EBPβ to three enhancer elements with different C/EBPβ motives.

(B) Activity reporter assay of different *Nr4a1* enhancer elements cloned in front of a luciferase gene. The constructs were transfected into MEF *Cebpb*$^{-/-}$ cells, which further received by transfection either 100ng control or C/EBPβ-containing plasmids. Shown is one experiment out of four with similar results.

REFERENCES

Alder, J.K., Georgantas, R.W., Hildreth, R.L., Kaplan, I.M., Morisot, S., Yu, X., McDevitt, M., and Civin, C.I. (2008). Kruppel-like factor 4 is essential for inflammatory monocyte differentiation in vivo. J. Immunol. *180*, 5645–5652.

Askenase, M.H., Han, S.J., Byrd, A.L., Morais da Fonseca, D., Bouladoux, N., Wilhelm, C., Konkel, J.E., Hand, T.W., Lacerda-Queiroz, N., Su, X.Z., et al. (2015). Bone-Marrow-Resident NK Cells Prime Monocytes for Regulatory Function during Infection. Immunity. 42, 1130-42.

Auffray, C., Fogg, D., Garfa, M., Elain, G., Join-Lambert, O., Kayal, S., Sarnacki, S., Cumano, A., Lauvau, G., and Geissmann, F. (2007). Monitoring of blood vessels and tissues by a population of monocytes with patrolling behavior. Science *317*, 666–670.

Bain, C.C., Hawley, C.A., Garner, H., Scott, C.L., Schridde, A., Steers, N.J., Mack, M., Joshi, A., Guilliams, M., Mowat, A.M.I., et al. (2016). Long-lived self-renewing bone marrow-derived macrophages displace embryo-derived cells to inhabit adult serous cavities. Nature Communications *7*, ncomms11852.

Bégay, V., Smink, J.J., Loddenkemper, C., Zimmermann, K., Rudolph, C., Scheller, M., Steinemann, D., Leser, U., Schlegelberger, B., Stein, H., et al. (2015). Deregulation of the endogenous C/EBPβ LIP isoform predisposes to tumorigenesis. J. Mol. Med. *93*, 39–49.

Bornstein, C., Winter, D., Barnett-Itzhaki, Z., David, E., Kadri, S., Garber, M., and Amit, I. (2014). A negative feedback loop of transcription factors specifies alternative dendritic cell chromatin States. Molecular Cell *56*, 749–762.

Buenrostro, J.D., Giresi, P.G., Zaba, L.C., Chang, H.Y., and Greenleaf, W.J. (2013). Transposition of native chromatin for fast and sensitive epigenomic profiling of open chromatin, DNA-binding proteins and nucleosome position. Nature Methods *10*, 1213–1218.

Carlin, L.M., Stamatiades, E.G., Auffray, C., Hanna, R.N., Glover, L., Vizcay-Barrena, G., Hedrick, C.C., Cook, H.T., Diebold, S., and Geissmann, F. (2013). Nr4a1-dependent Ly6C(low) monocytes monitor endothelial cells and orchestrate their disposal. Cell *153*, 362–375.

Creyghton, M.P., Cheng, A.W., Welstead, G.G., Kooistra, T., Carey, B.W., Steine, E.J., Hanna, J., Lodato, M.A., Frampton, G.M., Sharp, P.A., et al. (2010). Histone H3K27ac separates active from poised enhancers and predicts developmental state. Proc. Natl. Acad. Sci. U.S.a. *107*, 21931–21936.

Descombes, P., and Schibler, U. (1991). A liver-enriched transcriptional activator protein, LAP, and a transcriptional inhibitory protein, LIP, are translated from the same mRNA. Cell *67*, 569–579.

El-Asmar, B., Giner, X.C., and Tremblay, J.J. (2009). Transcriptional cooperation between NF-kappaB p50 and CCAAT/enhancer binding protein beta regulates Nur77 transcription in Leydig cells. J. Mol. Endocrinol. *42*, 131–138.

Feinberg, M.W., Wara, A.K., Cao, Z., Lebedeva, M.A., Rosenbauer, F., Iwasaki, H., Hirai, H., Katz, J.P., Haspel, R.L., Gray, S., et al. (2007). The Kruppel-like factor KLF4 is a critical regulator of monocyte differentiation. Embo J. *26*, 4138–4148.

Fogg, D.K., Sibon, C., Miled, C., Jung, S., Aucouturier, P., Littman, D.R., Cumano, A., and Geissmann, F. (2006). A clonogenic bone marrow progenitor specific for macrophages and dendritic cells. Science *311*, 83–87.

Geissmann, F., Jung, S., and Littman, D.R. (2003). Blood monocytes consist of two principal subsets with distinct migratory properties. Immunity *19*, 71–82.

Ginhoux, F., and Jung, S. (2014). Monocytes and macrophages: developmental pathways and tissue homeostasis. Nat. Rev. Immunol. *14*, 392–404.

Gren, S.T., Rasmussen, T.B., Janciauskiene, S., Håkansson, K., Gerwien, J.G., and Grip, O. (2015). A Single-Cell Gene-Expression Profile Reveals Inter-Cellular Heterogeneity within Human Monocyte Subsets. PLoS ONE *10*, e0144351.

Haghverdi, L., Buettner, F., and Theis, F.J. (2015). Diffusion maps for high-dimensional single-cell analysis of differentiation data. Bioinformatics *31*, 2989–2998.

Hanna, R.N., Carlin, L.M., Hubbeling, H.G., Nackiewicz, D., Green, A.M., Punt, J.A., Geissmann, F., and Hedrick, C.C. (2011). The transcription factor NR4A1 (Nur77) controls bone marrow differentiation and the survival of Ly6C- monocytes. Nat. Immunol. *12*, 778–785.

Heintzman, N.D., Stuart, R.K., Hon, G., Fu, Y., Ching, C.W., Hawkins, R.D., Barrera, L.O., Van Calcar, S., Qu, C., Ching, K.A., et al. (2007). Distinct and predictive chromatin signatures of transcriptional promoters and enhancers in the human genome. Nat. Genet. *39*, 311–318.

Hettinger, J., Richards, D.M., Hansson, J., Barra, M.M., Joschko, A.-C., Krijgsveld, J., and Feuerer, M. (2013). Origin of monocytes and macrophages in a committed progenitor. Nat. Immunol. *14*, 821–830.

Jaitin, D.A., Kenigsberg, E., Keren-Shaul, H., Elefant, N., Paul, F., Zaretsky, I., Mildner, Cohen, N., Jung, S., Tanay, A., et al. (2014). Massively parallel single-cell RNA-seq for marker-free decomposition of tissues into cell types. Science *343*, 776–779.

Kim, K.-W., Williams, J.W., Wang, Y.-T., Ivanov, S., Gilfillan, S., Colonna, M., Virgin, H.W., Gautier, E.L., and Randolph, G.J. (2016). MHC II+ resident peritoneal and pleural macrophages rely on IRF4 for development from circulating monocytes. J. Exp. Med. *213*, 1951–1959.

Kurotaki, D., Osato, N., Nishiyama, A., Yamamoto, M., Ban, T., Sato, H., Nakabayashi, J., Umehara, M., Miyake, N., Matsumoto, N., et al. (2013). Essential role of the IRF8-KLF4 transcription factor cascade in murine monocyte differentiation. Blood *121*, 1839–1849.

Lara-Astiaso, D., Weiner, A., Lorenzo-Vivas, E., Zaretsky, I., Jaitin, D.A., David, E., Keren-Shaul, H., Mildner, Winter, D., Jung, S., et al. (2014). Immunogenetics. Chromatin state dynamics during blood formation. Science *345*, 943–949.

Lavin, Y., Winter, D., Blecher-Gonen, R., David, E., Keren-Shaul, H., Merad, M., Jung, S., and Amit, I. (2014). Tissue-resident macrophage enhancer landscapes are shaped by the local microenvironment. Cell *159*, 1312–1326.

Leutz, A., Pless, O., Lappe, M., Dittmar, G., and Kowenz-Leutz, E. (2011). Crosstalk between phosphorylation and multi-site arginine/lysine methylation in C/EBPs. Transcription *2*, 3–8.

Menezes, S., Melandri, D., Anselmi, G., Perchet, T., Loschko, J., Dubrot, J., Patel, R., Gautier, E.L., Hugues, S., Longhi, M.P., et al. (2016). The Heterogeneity of Ly6C(hi) Monocytes Controls Their Differentiation into iNOS(+) Macrophages or Monocyte-Derived Dendritic Cells. Immunity *45*, 1205–1218.

Mildner, A., Yona, S., and Jung, S. (2013). A close encounter of the third kind: monocyte-derived cells. Adv. Immunol. *120*, 69–103.

Molawi, K., Wolf, Y., Kandalla, P.K., Favret, J., Hagemeyer, N., Frenzel, K., Pinto, A.R., Klapproth, K., Henri, S., Malissen, B., et al. (2014). Progressive replacement of embryo-derived cardiac macrophages with age. J. Exp. Med. *211*, 2151–2158.

Palframan, R.T., Jung, S., Cheng, G., Weninger, W., Luo, Y., Dorf, M., Littman, D.R., Rollins, B.J., Zweerink, H., Rot, A., et al. (2001). Inflammatory chemokine transport and presentation in HEV: a remote control mechanism for monocyte recruitment to lymph nodes in inflamed tissues. J. Exp. Med. *194*, 1361–1373.

Passlick, B., Flieger, D., and Ziegler-Heitbrock, H.W. (1989). Identification and characterization of a novel monocyte subpopulation in human peripheral blood. Blood *74*, 2527–2534.

Paul, F., Arkin, Y., Giladi, A., Jaitin, D.A., Kenigsberg, E., Keren-Shaul, H., Winter, D., Lara-Astiaso, D., Gury, M., Weiner, A., et al. (2015). Transcriptional Heterogeneity and Lineage Commitment in Myeloid Progenitors. Cell *163*, 1663–1677.

Schmidl, C., Renner, K., Peter, K., Eder, R., Lassmann, T., Balwierz, P.J., Itoh, M., Nagao-Sato, S., Kawaji, H., Carninci, P., et al. (2014). Transcription and enhancer profiling in human monocyte subsets. Blood *123*, e90–e99.

Scott, E.W., Simon, M.C., Anastasi, J., and Singh, H. (1994). Requirement of transcription factor PU.1 in the development of multiple hematopoietic lineages. Science *265*, 1573–1577.

Serbina, N.V., and Pamer, E.G. (2006). Monocyte emigration from bone marrow during bacterial infection requires signals mediated by chemokine receptor CCR2. Nat. Immunol. *7*, 311–317.

Smink, J.J., Bégay, V., Schoenmaker, T., Sterneck, E., de Vries, T.J., and Leutz, A. (2009). Transcription factor C/EBPbeta isoform ratio regulates osteoclastogenesis through MafB. Embo J. *28*, 1769–1781.

Srinivas, S., Watanabe, T., Lin, C.S., William, C.M., Tanabe, Y., Jessell, T.M., and Costantini, F. (2001). Cre reporter strains produced by targeted insertion of EYFP and ECFP into the ROSA26 locus. BMC Dev. Biol. *1*, 4.

Sugimoto, C., Hasegawa, A., Saito, Y., Fukuyo, Y., Chiu, K.B., Cai, Y., Breed, M.W., Mori, K., Roy, C.J., Lackner, A.A., et al. (2015). Differentiation Kinetics of Blood Monocytes and Dendritic Cells in Macaques: Insights to Understanding Human Myeloid Cell Development. The Journal of Immunology *195*, 1774–1781.

Sunderkötter, C., Nikolic, T., Dillon, M.J., Van Rooijen, N., Stehling, M., Drevets, D.A., and Leenen, P.J.M. (2004). Subpopulations of mouse blood monocytes differ in maturation stage and inflammatory response. J. Immunol. *172*, 4410–4417.

Tamoutounour, S., Guilliams, M., Sanchis, F.M., Liu, H., Terhorst, D., Malosse, C., Pollet, E., Ardouin, L., Luche, H., Sanchez, C., et al. (2013). Origins and Functional Specializationof Macrophages and of Conventionaland Monocyte-Derived Dendritic Cells in Mouse Skin. Immunity *39*, 925–938.

Tamura, A., Hirai, H., Yokota, A., Sato, A., Shoji, T., Kashiwagi, T., Iwasa, M., Fujishiro, A., Miura, Y., and Maekawa, T. (2015). Accelerated apoptosis of peripheral blood monocytes in Cebpb-deficient mice. Biochemical and Biophysical Research Communications *464*, 654–658.

Varol, C., Landsman, L., Fogg, D.K., Greenshtein, L., Gildor, B., Margalit, R., Kalchenko, V., Geissmann, F., and Jung, S. (2007). Monocytes give rise to mucosal, but not splenic, conventional dendritic cells. J. Exp. Med. *204*, 171–180.

Varol, C., Vallon-Eberhard, A., Elinav, E., Aychek, T., Shapira, Y., Luche, H., Fehling, H.J., Hardt, W.-D., Shakhar, G., and Jung, S. (2009). Intestinal lamina propria dendritic cell subsets have different origin and functions. Immunity *31*, 502–512.

Wethmar, K., Bégay, V., Smink, J.J., Zaragoza, K., Wiesenthal, V., Dörken, B., Calkhoven, C.F., and Leutz, A. (2010). C/EBPbetaDeltauORF mice--a genetic model for uORF-mediated translational control in mammals. Genes & Development *24*, 15–20.

Wong, K.L., Yeap, W.-H., Tai, J.J.-Y., Ong, S.M., Dang, T.M., and Wong, S.-C. (2012). The three human monocyte subsets: implications for health and disease. Immunol. Res. *53*, 41–57.

Yona, S., Kim, K.-W., Wolf, Y., Mildner, Varol, D., Breker, M., Strauss-Ayali, D., Viukov, S., Guilliams, M., Misharin, A., et al. (2013). Fate mapping reveals origins and dynamics of monocytes and tissue macrophages under homeostasis. Immunity *38*, 79–91.

Zawada, A.M., Rogacev, K.S., Rotter, B., Winter, P., Marell, R.-R., Fliser, D., and Heine, G.H. (2011). SuperSAGE evidence for CD14++CD16+ monocytes as a third monocyte subset. Blood *118*, e50–e61.

.

Figure 1

Click here to download Figure Fig.1.jpg

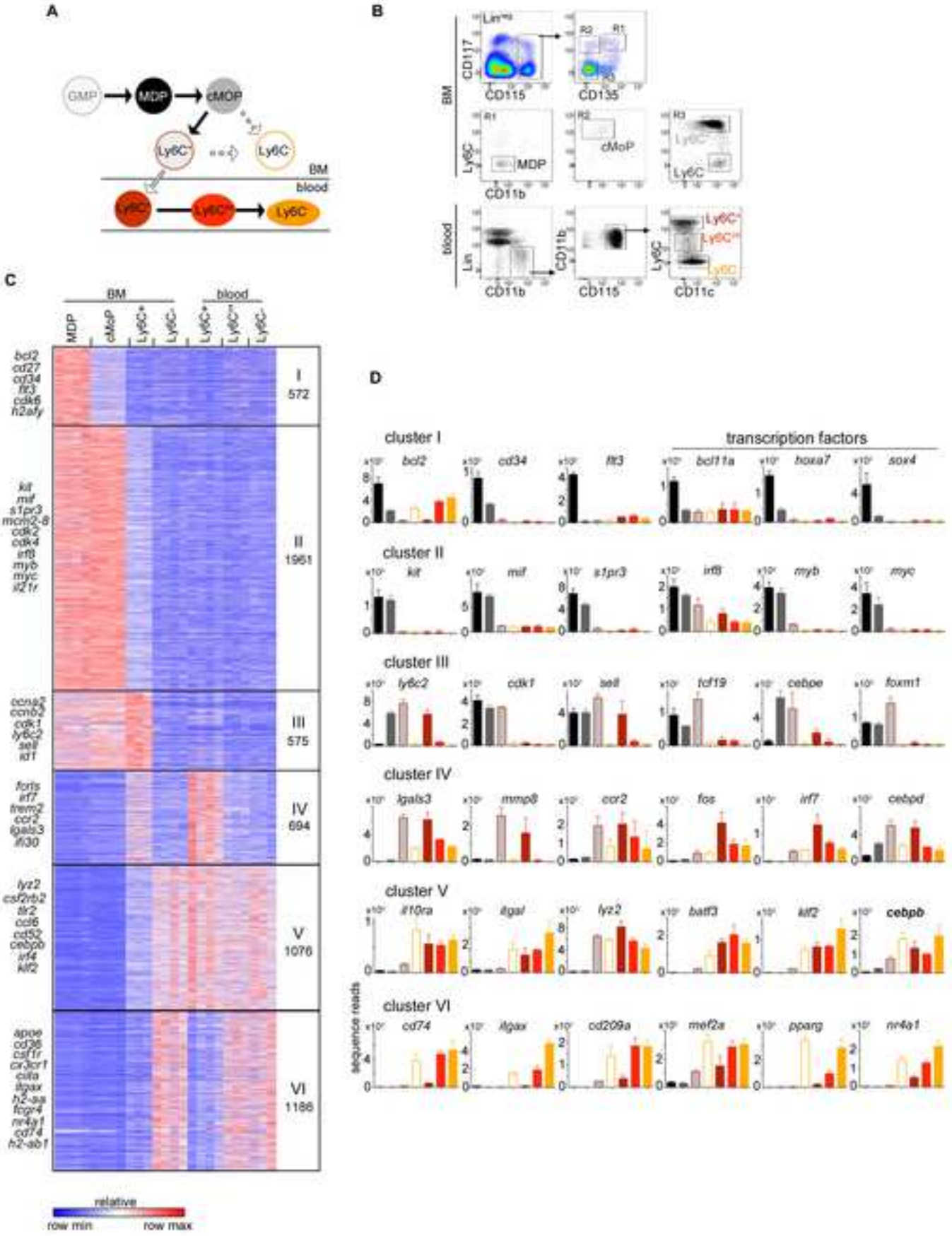

Figure 1

Figure 2

Click here to download Figure Fig.2.jpg

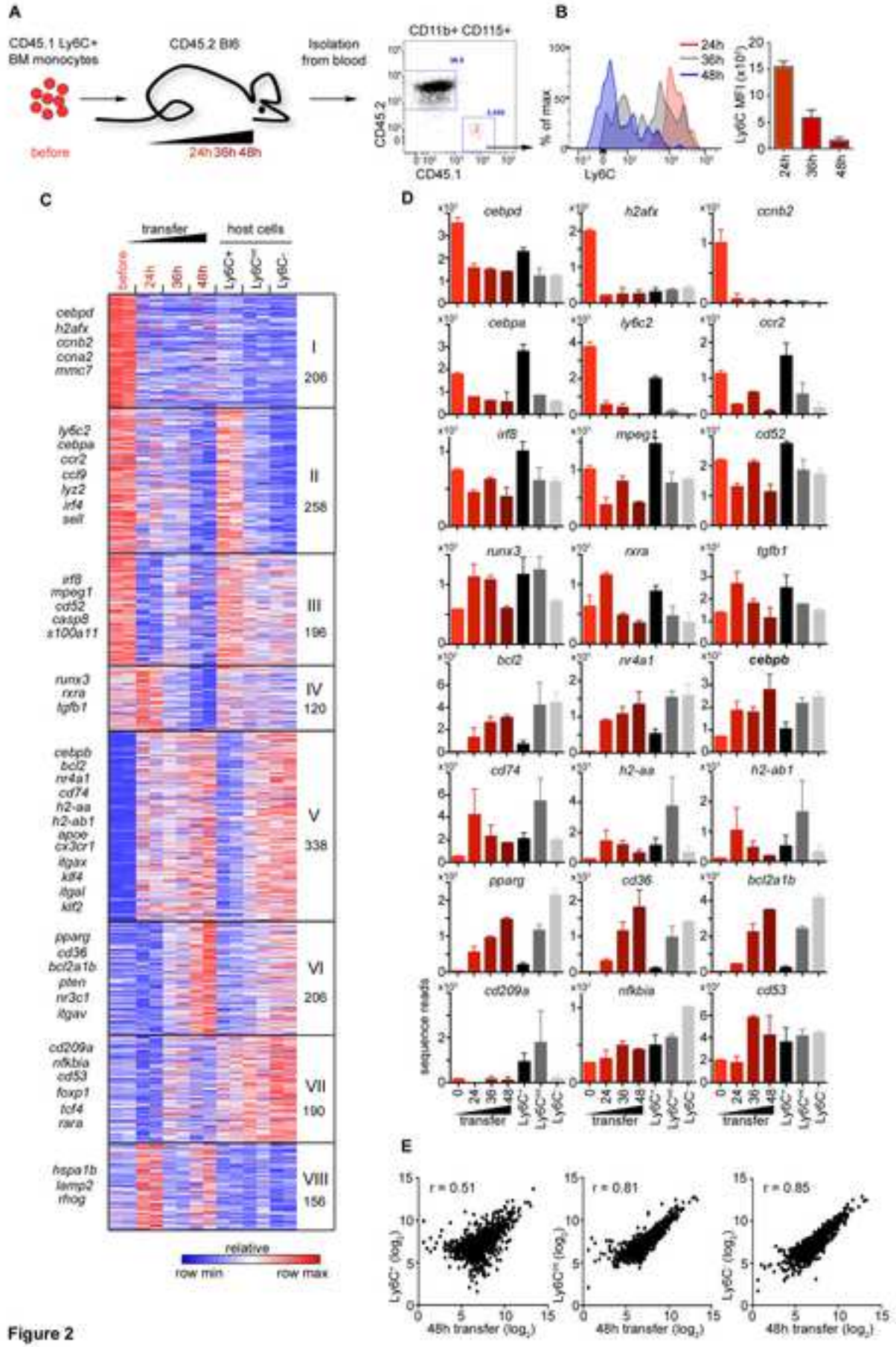

Figure 2

Figure 3

Click here to download Figure Fig.3x.jpg

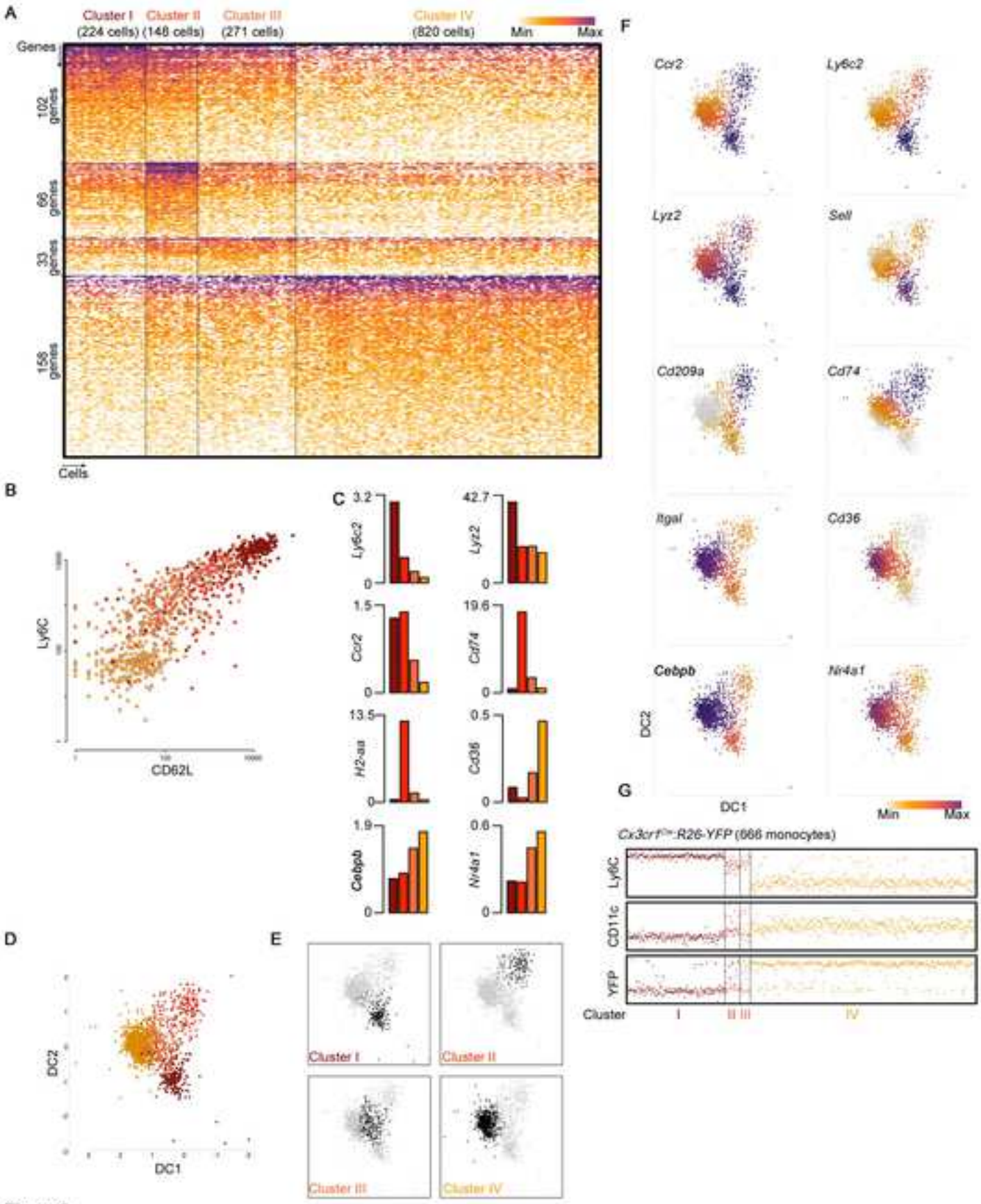

Figure 3

Figure 4

Click here to download Figure Fig.4.jpg

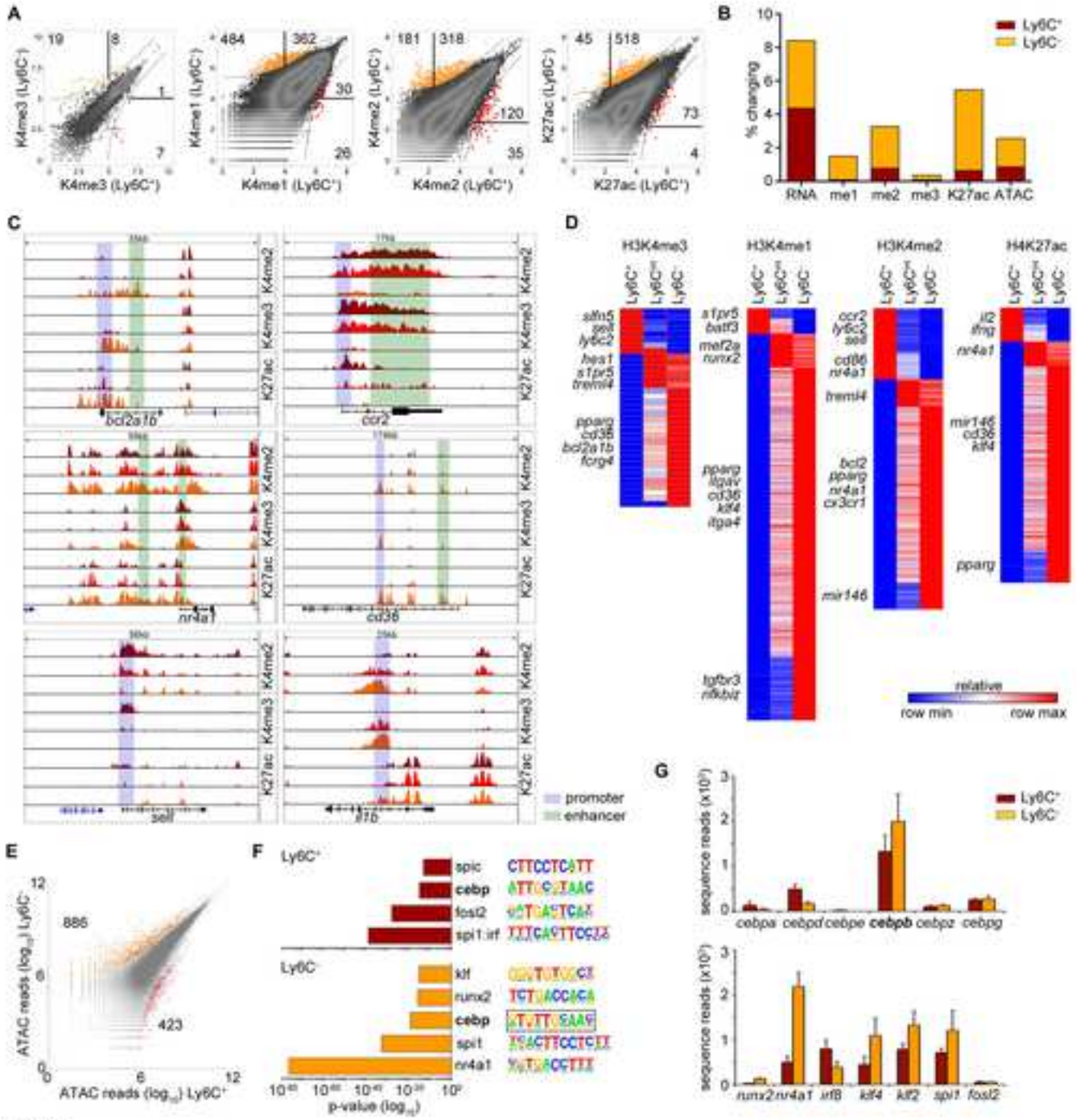

Figure 4

Click here to download Figure Fig.5.jpg

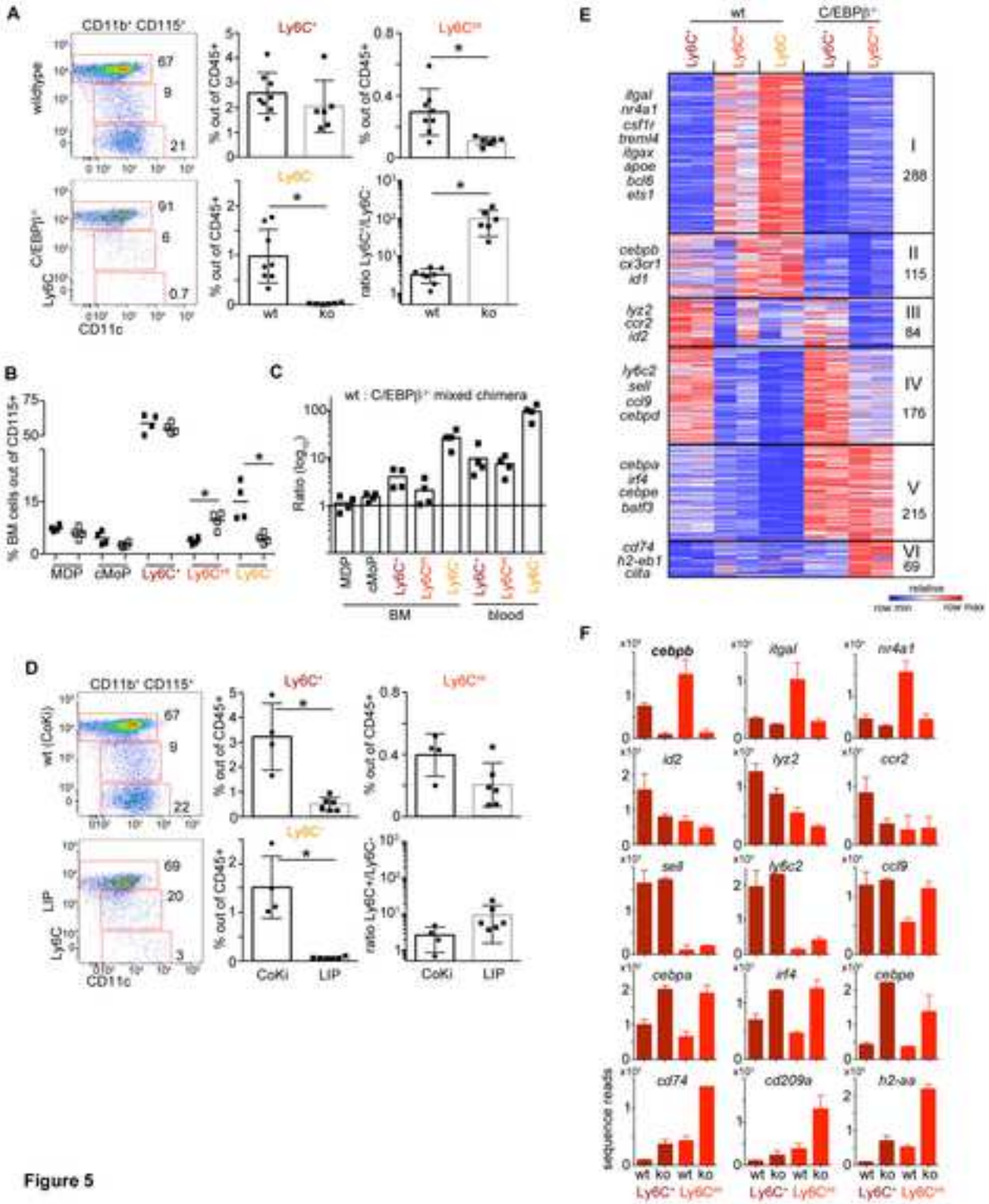

Figure 5

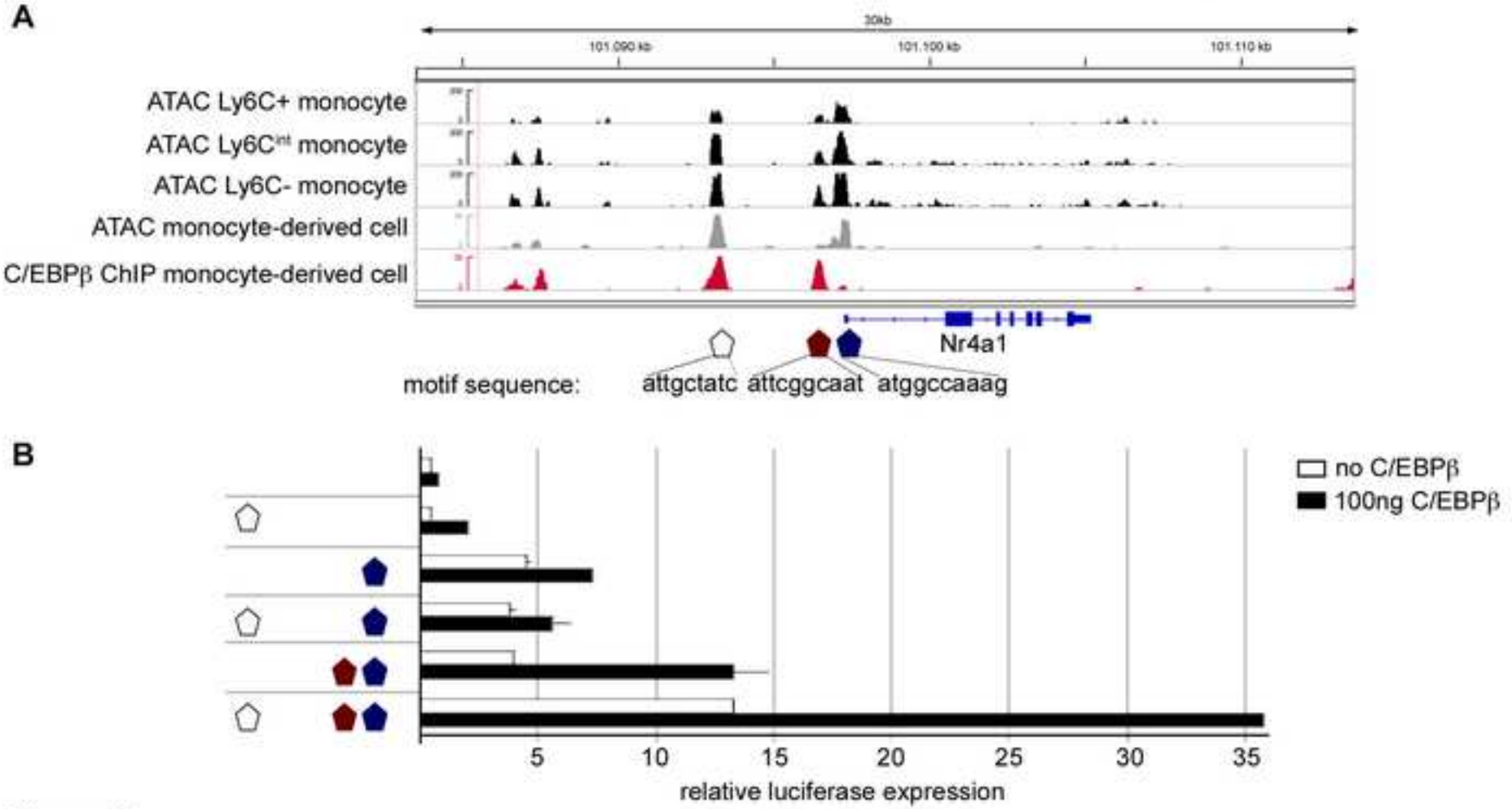

Figure 6

KEY RESOURCES TABLE

REAGENT or RESOURCE	SOURCE	IDENTIFIER
Antibodies		
Anti-Ly6C FITC (clone HK1.4)	Biolegend	Cat# 128006 RRID:AB_1186135
Anti-Ly6C PerCP-Cy5.5 (clone HK1.4)	eBioscience	Cat# 45-5932 RRID:AB_1518763
Anti-Ly6C APC (clone HK1.4)	Biolegend	Cat# 128016 RRID:AB_1732076
Anti-Ly6C APC-Cy7 (clone HK1.4)	Biolegend	Cat# 128025 RRID:AB_10643867
Anti-CD11c APC (clone N418)	Biolegend	Cat# 117310 RRID:AB_313779
Anti-CD11c PE (clone N418)	Biolegend	Cat# 117307 RRID:AB_313776
Anti-CD115 Biotin (clone AFS98)	Biolegend	Cat# 135507 RRID:AB_2028401
Anti-CD115 PE (clone AFS98)	Biolegend	Cat# 135507 RRID:AB_1937253
Anti-CD115 PE-Cy7 (clone AFS98)	Biolegend	Cat# 135524 RRID:AB_2566460
Anti-CD45.2 Pacific Blue (clone 104)	Biolegend	Cat# 109820 RRID:AB_492872
Anti-CD45.2 FITC (clone 104)	Biolegend	Cat# 109806 RRID:AB_313443
Anti-CD45.1 PE (clone A20)	Biolegend	Cat# 110707 RRID:AB_313496
Anti-CD45.1 APC (clone A20)	Biolegend	Cat# 110714 RRID:AB_313503
Anti-CD3e BV421 (clone 145-2C11)	Biolegend	Cat# 100335 RRID:AB_10898314
Anti-TCRgd BV421 (clone GL3)	Biolegend	Cat# 118119 RRID:AB_10896753
Anti-Ly6G BV421 (clone 1A8)	Biolegend	Cat# 127627 RRID:AB_10897944
Anti-Nk1.1 BV421 (clone PK136)	Biolegend	Cat# 108732 RRID:AB_2562218
Anti-B220 BV421 (clone RA3-6B2)	Biolegend	Cat# 103240 RRID:AB_11203896
Anti-CD19 BV421 (clone 6D5)	Biolegend	Cat# 115538 RRID:AB_11203527
Anti-Ter119 BV421 (clone TER119)	Biolegend	Cat# 116234 RRID:AB_2562917
Anti-CD11b APC (clone M1/70)	Biolegend	Cat# 101211 RRID:AB_312794
Anti-CD11b PerCP-Cy5.5 (clone M1/70)	Biolegend	Cat# 101228 RRID:AB_893232
Anti-CD11b PE-Cy7 (clone M1/70)	Biolegend	Cat# 101215 RRID:AB_312798
Anti-CD135 Biotin (clone A2F10)	eBioscience	Cat# 13-1351-81 RRID:AB_466598
Anti-CD62L PE (clone MEL-14)	eBioscience	Cat# 12-0621-81 RRID:AB_465720

Anti-CD117 PE/Cy7 (clone 2B8)	Biolegend	Cat# 105813 RRID:AB_313222
Anti-I-Ab PE/Cy7 (clone AF6-120.1)	Biolegend	Cat# 116420 RRID:AB_10575296
Anti-I-Ab PerCP-Cy5.5 (clone AF6-120.1)	Biolegend	Cat# 116416 RRID:AB_1953309
Anti-Ly6G APC-Cy7 (clone 1A8)	Biolegend	Cat# 127623 RRID:AB_10645331
Anti-B220 FITC (clone RA3-6B2)	Biolegend	Cat# 103206 RRID:AB_312991
Anti-B220 APC (clone RA3-6B2)	Biolegend	Cat# 103211 RRID:AB_312996
Anti-CD4 APC (clone GK1.5)	Biolegend	Cat# 100411 RRID:AB_312696
Anti-CD8a APC (clone 53-6.7)	eBioscience	Cat# 17-0081-82 RRID:AB_469335
Anti-Ly6G APC (clone 1A8)	eBioscience	Cat# 17-9668-80 RRID:AB_2573306
Anti-Nk1.1 APC (clone PK136)	eBioscience	Cat# 17-5941-63 RRID:AB_469477
Anti-TCRgd APC (clone GL3)	Biolegend	Cat# 118116 RRID:AB_1731813
Anti-biotin MicroBeads	Miltenyi	Cat# 130-090-485 RRID:AB_244365
Anti-H3K27ac antibody	Abcam	Cat# ab4729 RRID:AB_2118291
Anti-Histone H3 (tri methyl K4) antibody	Millipore	Cat# 07-473 RRID:AB_1977252
Anti-Histone H3 (di methyl K4) antibody	Abcam	Cat# ab32356 RRID:AB_732924
Anti-Histone H3 (mono methyl K4) antibody	Abcam	Cat# ab8895 RRID:AB_306847
Anti-Histone H3	Abcam	Cat# ab1791 RRID:AB_302613
Chemicals, Peptides, and Recombinant Proteins		
Dynabeads® Oligo(dT)25	ThermoFischer	Cat# 61005
Agencourt AMPure XP	Beckman Coulter	Cat# A63881
Exonuclease I	New England Biolabs	Cat# M0293L
NEBNext® mRNA Second Strand Synthesis Module	New England Biolabs	Cat# e6111L
RNA Fragmentation Reagents	ThermoFischer	Cat# AM8740
Turbo DNase I	ThermoFischer	Cat# AM2239
T4 RNA Ligase 1	New England Biolabs	Cat# M0204L
HiScribe™ T7 High Yield RNA Synthesis Kit	New England Biolabs	Cat# E2040
Kapa hifi PCR Kits	Kapabiosystems	Cat# KK2602
AffinityScript Multiple Temperature Reverse Transcriptase	Agilent	Cat# 600109
PowerUp™ SYBR® Green Master Mix	ThermoFischer	Cat# A25777
T4 Polynucleotide Kinase	New England Biolabs	Cat# M0201
cOmplete™ Protease Inhibitor Cocktail	Sigma-Aldrich	Cat# 11697498001
Dynabeads® Protein G	ThermoFisher	Cat# 1004D

Klenow Fragment (3'→ 5' exo-)	New England Biolabs	Cat# M0212
Proteinase K	New England Biolabs	Cat# P8102
RNaseA	Roche	Cat# 11119915001
PE/Cy7 Streptavidin	BioLegend	Cat# 405206
BV605 Streptavidin	Biolegend	Cat# 405229
Critical Commercial Assays		
Quick Ligation™ Kit	New England Biolabs	Cat# M2200
Amicon Ultra-15	Merck	Cat# UFC905024
Nextera Sample Preparation Kit	Illumina	Cat# FC-121-1030
Deposited Data		
RAW and analysed data	GEO	GSE95702
Experimental Models: Organisms/Strains		
Mouse: *Cx3cr1*-Cre	Laboratory of S. Jung	Yona et al., 2013
Mouse: *Cebpb*$^{-/-}$	Laboratory of R.C. Smart	Sterneck et al., 2006
Mouse: LIP	Laboratory of A. Leutz	Bégay et al., 2015
Mouse: CoKi	Laboratory of A. Leutz	Wethmar et al., 2010
Mouse: RosaYFP	Laboratory of F. Costantini	Srinivas et al., 2001
Mouse: CD45.2 (WT)	Harlan	Stock: B6.Cg.129P2
Mouse: CD45.1	Harlan	Stock: B6.SJL-PtprcaPep3b/BoyJ
Oligonucleotides		
ChIP Universal Adaptor	5'ACACTCTTTCCCTACACGACGCTCTTCCGATC*T-3′ , where * indicates phosphothionate modification.	
ChIP Indexed Adaptor	5'GATCGGAAGAGCACACGTCTGAACTCCAGTCACXXXXXXATCTCGTATGCCGTCTTCTGTT- 3', where XXXXXX is the barcode for sample multiplexing	
Y- Shaped Indexed adaptors	Anneal ssUniversal Adaptor and ssIndexed Adaptors to obtain Y-shaped Indexed Adaptors.	
ChIP PCR for	5'-AATGATACGGCGACCACCGAGATCTACACTCTTTCCCTACACGAC-3′	
ChIP PCR rec	5'-CAAGCAGAAGACGGCATACGAGAT-3′	
MARS-Seq barcoded RT primer	CGATTGAGGCCGGTAATACGACTCACTATAGGGGCGACGTGTGCTCTTCCGATCTXXXXXXNNNNTTTTTTTTTTTTTTTTTTTTTN, where XXXXXX is the	
MARS-Seq ligation primer	AGATCGGAAGAGCGTCGTGTAG, modified with a phosphate group at 5' and a C3 spacer (blocker) at the 3'	
MARS-Seq 2nd RT primer	TCTAGCCTTCTCGCAGCACATC	

MARS-Seq P5_Rd1 PCR forward	AATGATACGGCGACCACCGAGATCTACACTCTTTCCCTACACGACGC TCTTCCGATCT	
MARS-Seq P7_Rd2 PCR reverse	CAAGCAGAAGACGGCATACGAGATGTGACTGGAGTTCAGACGTGTG CTCTTCCGATCT	
Recombinant DNA		
pcDNA3.1	Addgene	
pGL4.10	Promega	Cat# E665A
pGL4.70	Promega	Cat# E6881
Software and Algorithms		
GraphPad Prism 6	GraphPad Software, Inc., Carlifornia	
FlowJo 8.7	TreeStar; FlowJo LLC; Ashland, Oregon	
MarkDuplicates	http://broadinstitute.github.io/picard/	
Bowtie2 aligner version 2.2.5	http://bowtie-bio.sourceforge.net/bowtie2/index.shtml	
HOMER	http://homer.ucsd.edu/homer/introduction/install.html	
DAVID	https://david.ncifcrf.gov/	
HISAT	https://ccb.jhu.edu/software/hisat/index.shtml	
Picard	http://broadinstitute.github.io/picard/	
Other		
multinomial mixture-model algorithm	this study	http://compgenomics.weizmann.ac.il/tanay/?page_id=649

SUPPLEMENTARY Table legends

Supplementary Table 1. Core gene expression in the identified four clusters by single cell RNA-Seq. Supporting text figure 3.

Supplementary Table 2. Promoter and enhancer changes in Ly6C^{+}, Ly6C^{int} and Ly6C^{-} monocytes. Supporting text figure 4.

Full list of H3K4me1, H3K4me2, H3K4me3 and H3K27ac changes in the three monocyte populations as identified and depicted in the X/Y graphs of Fig. 4A.

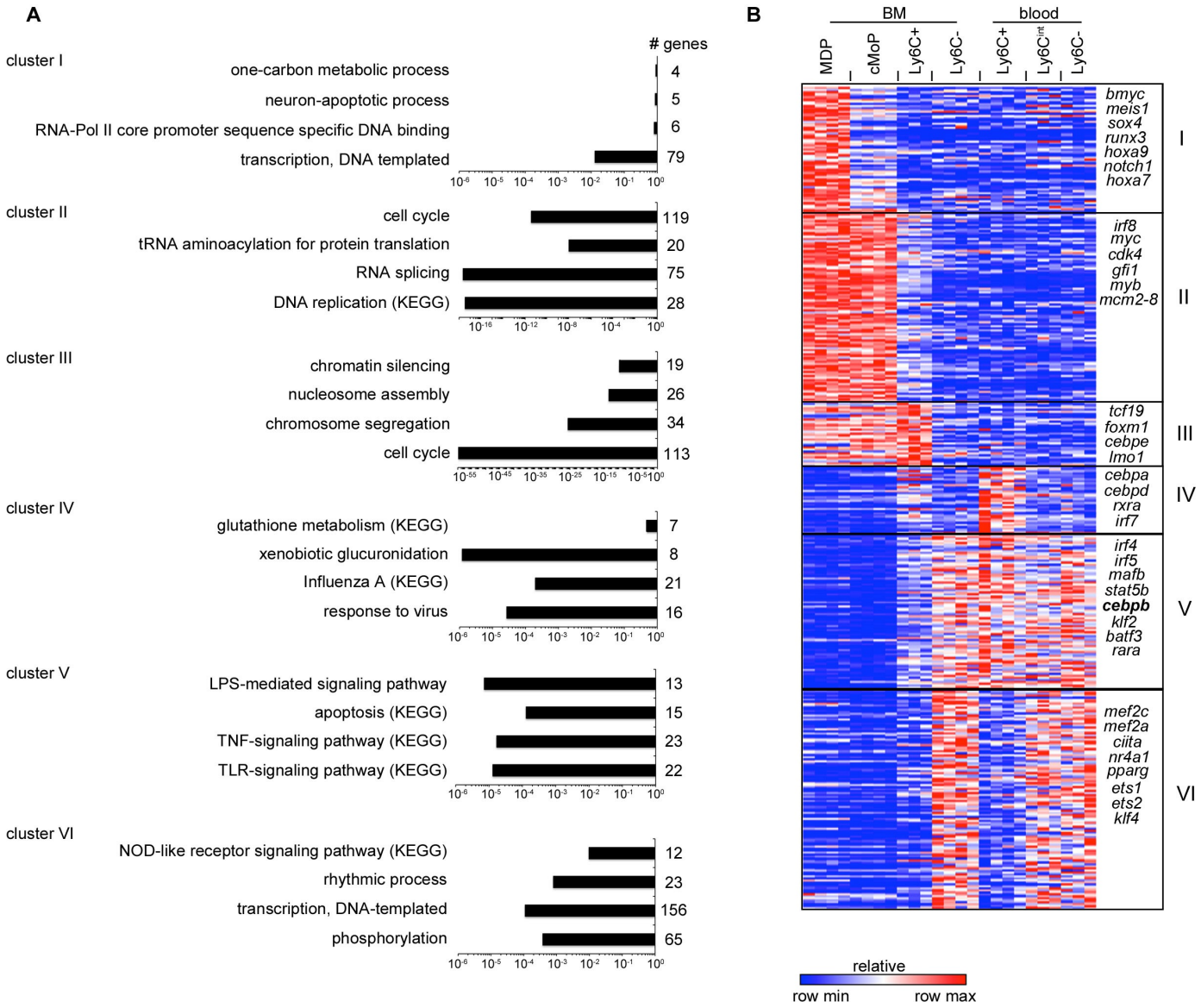

Supplementary Figure 1. GO-enrichment and TF expression in monocytes and their precursors. Supporting main text figure 1.

(A) P-values of selected GO-enrichment in the six clusters depicted in **Fig. 1C**. Significant changes in GO terms (biological processes) and in KEGG pathways are shown. Redundant or overlapping enrichments were not depicted.

(B) Transcription factor expression in the six clusters depicted in **Fig. 1C**. TF were taken from the riken website (http://genome.gsc.riken.jp/TFdb/tf_list.html) and from http://www.tfcat.ca/index.php.

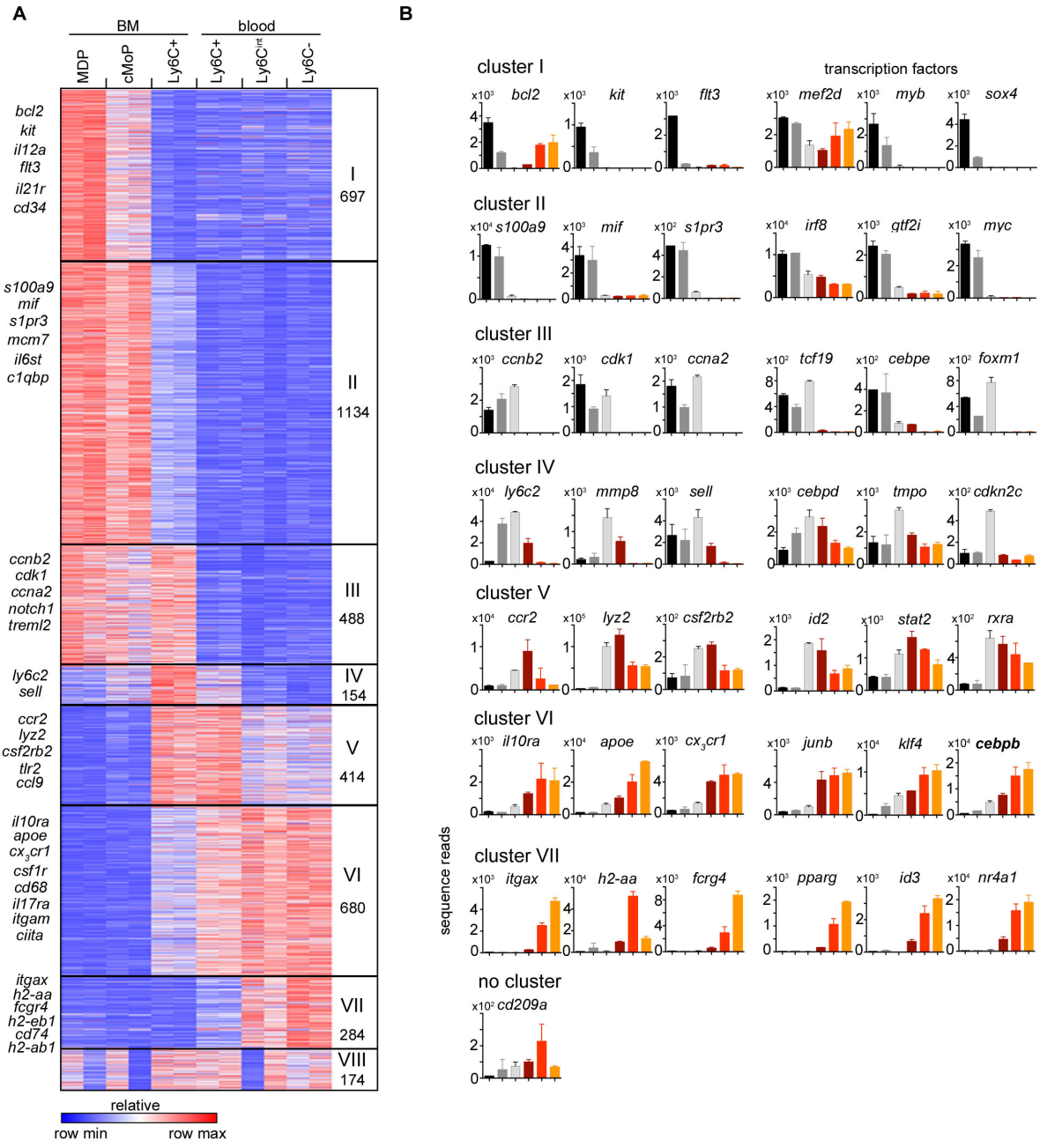

Supplementary Figure 2. Independent monocyte profiling by RNA-Seq
Supporting main text figure 1.

(A) Expression analysis of an additional set of murine MDP, cMoP, BM Ly6C+ monocytes and the three circulating blood monocyte subsets Ly6C+, Ly6Cint and Ly6C- by RNA-Seq. Samples were analyzed in duplicates and analysis was restricted to genes, which showed a 2-fold difference in at least one cell population and sample. K-means clustering was set to n = 8.

(B) Examples of gene expression from the eight identified clusters depicted in C. Shown are the mean sequence reads ± STD. Note that *cd209a* and MHCII-related gene expression was in this experiment restricted to Ly6C^{int} monocytes and not expressed by Ly6C^{-} monocytes.
Supporting main text figure 1.

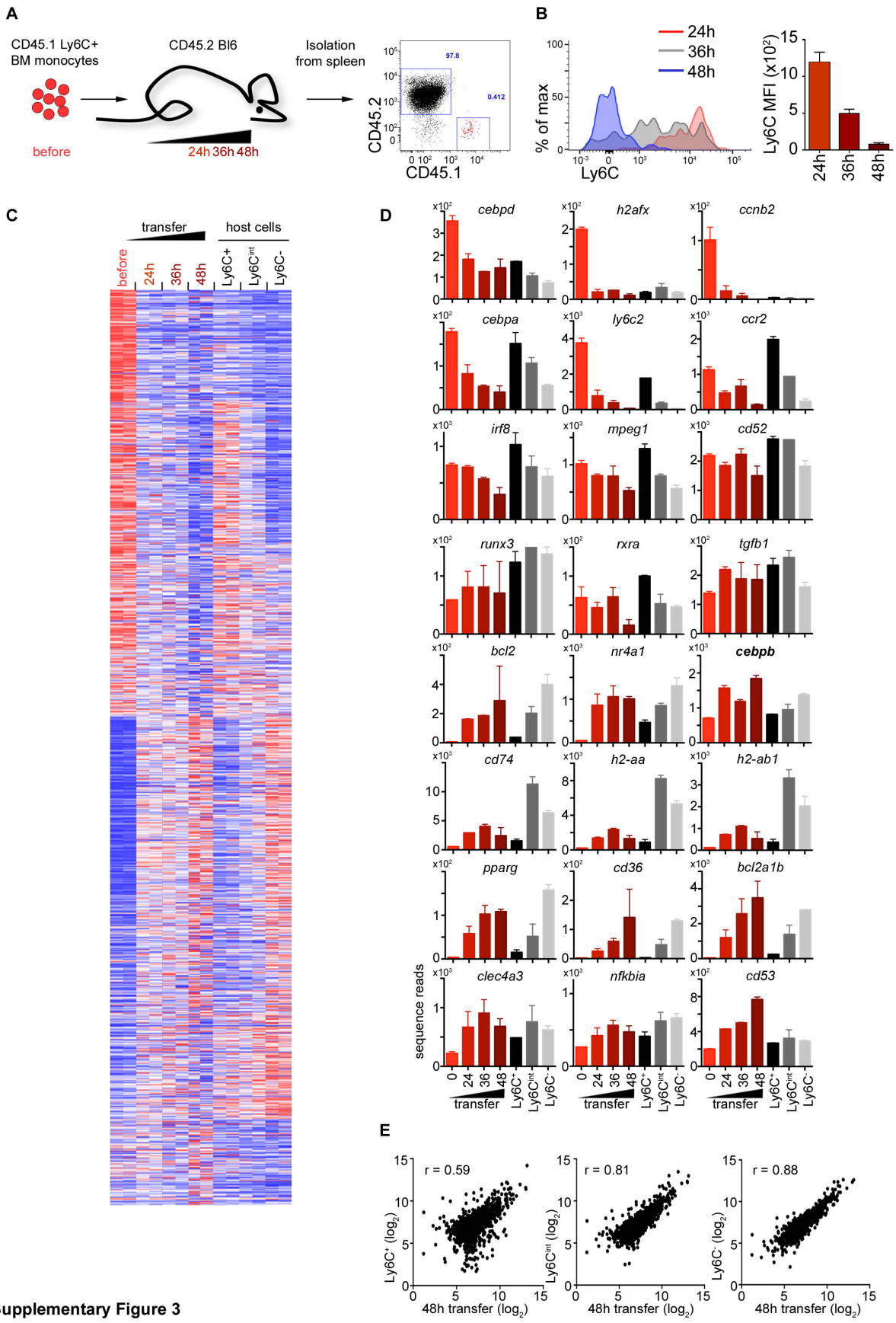

Supplementary Figure 3

Supplementary Figure 3. Transferred BM Ly6C$^+$ monocytes develop on the molecular level into splenic Ly6C$^-$ monocytes. Supporting main text figure 2.

(A) Schematic view of monocyte transfer experiment. CD45.1$^+$ Ly6C$^+$ BM monocytes were purified by FACS sorting and 2x10^5 cells were injected into CD45.2 congenic mice. 24h, 36h and 48h hours after injection, the transferred CD45.1$^+$ CD11b$^+$ CD115$^+$ monocytes were re-isolated from the spleen by FACS sorting and analyzed by RNA-Seq. Splenic Ly6C$^+$, Ly6C^{int} and Ly6C$^-$ monocytes from the host mice were analyzed by RNA-Seq in parallel and served as control.

(B) Histogram (left panel) and mean fluorescence intensity (MFI; right panel) of Ly6C expression on transferred splenic monocytes 24h (red), 36h (grey) and 48h (blue) hours after injection. Two recipients per time point were analyzed and the mean MFI ± STD are shown.

(C) Expression analysis of transferred monocytes from the spleen before, 24h, 36h and 48h after injection as well as host splenic Ly6C$^+$, Ly6C^{int} and Ly6C$^-$ monocyte subsets by RNA-Seq. We used the same clustering as shown in **Fig. 2C** to indicate overlapping transcriptional regulation in both organs.

(D) Examples of expression levels from individual genes identified by the cluster analysis depicted in C. Shown are the mean sequence reads ± STD.

(E) Correlation analysis of the expression signature of splenic monocytes isolated 48h after transfer against host splenic Ly6C$^+$, Ly6C^{int} and Ly6C$^-$ monocyte subsets. The 1472 differential expressed genes without the BM-specific genes from C (cluster II-VIII) and the average of the duplicates were used for calculation. Sequence reads are presented as $\log_2$ values.

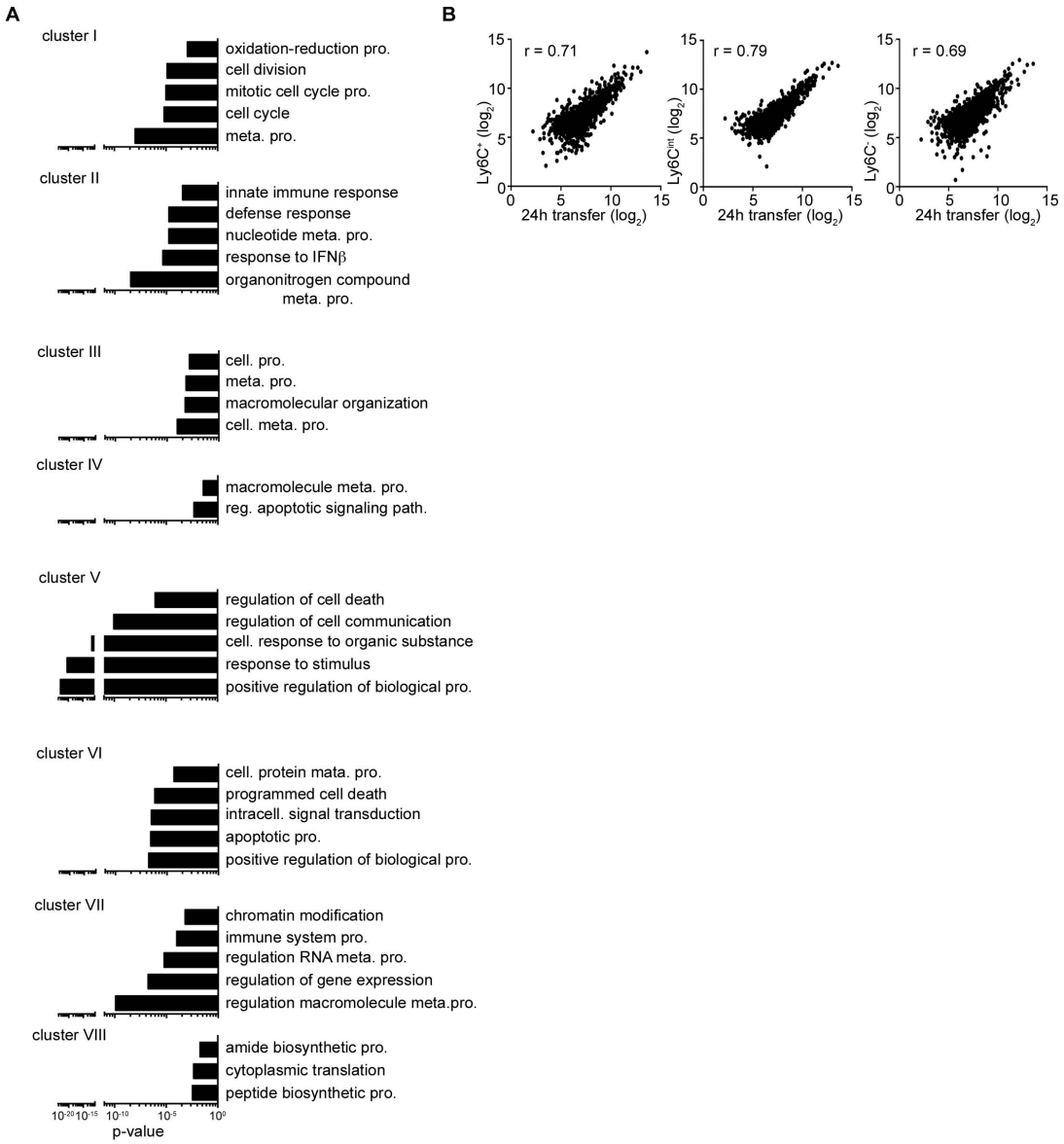

Supplementary Figure 4. GO-enrichment in host and transferred blood monocytes and conversion pattern of the 24h monocyte graft.

Supporting main text figure 2.

(A) P-values of selected GO-enrichment in the eight clusters depicted in **Fig. 2C**. The main GO terms belong to biological processes and cellular component. Redundant or overlapping enrichments were not depicted.

(B) Correlation analysis of the expression signature of monocytes isolated 24h after transfer against host Ly6C^{+}, Ly6C^{int} and Ly6C^{-} monocyte subsets. The 1472 differential expressed genes without the BM-specific cluster I from **Fig. 2C** were used (cluster II-VIII) and the average of the duplicates were used for calculation. Sequence reads are presented as $\log_2$ values.

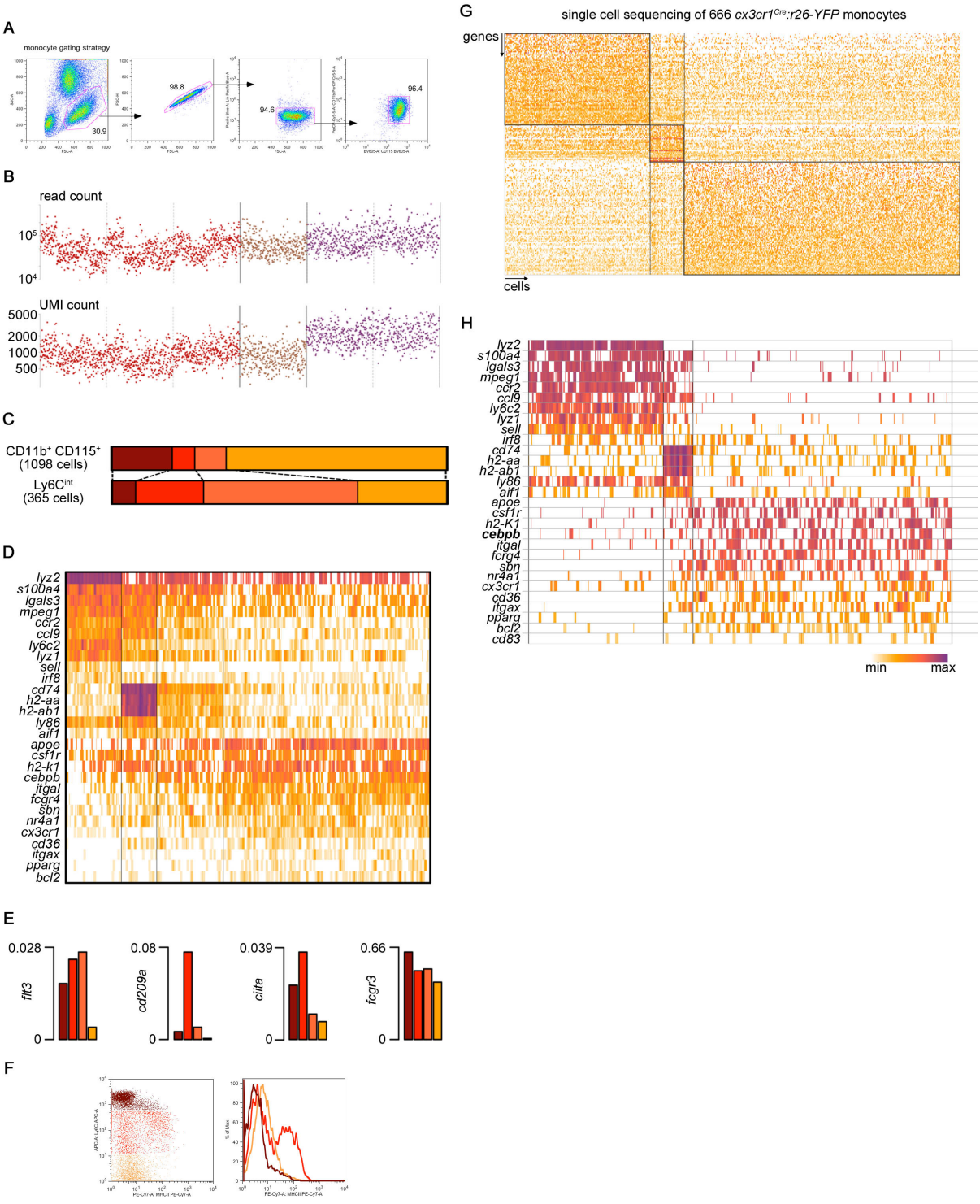

Supplementary Figure 5

Supplementary Figure 5. FACS gating strategy of monocytes for single cell RNA sequencing. Supporting main text figure 3.

(A) Monocytes were isolated from the blood of wt mice by CD115-biotin followed by anti-biotin MACS enrichment without red blood cell lysis. Cells were defined and sorted as lineage negative (B220, CD19, CD3, NK1.1, Ly6G, TCR$\gamma\delta$), $CD11b^+$ and $CD115^+$.

(B) Read and UMI count of the 1463 analyzed single cells.

(C) Distribution of the four clusters in the 1098 total monocytes (upper panel) and in the 365 $Ly6C^{int}$ cells.

(D) Detailed gene expression analysis of selected genes in the four clusters.

(E) Bar diagram of average gene expression in the four clusters. Note that *cd209a* was specifically expressed in cluster II cells. A full list of the detected genes as average in each cluster can be found in **Suppl. Tabl. 1**.

(F) FACS analysis of blood monocytes for MHCII (IA^b) expression. A small subset of $Ly6C^{int}$ monocytes express MHCII on their surface.

(G) Clustering of 666 monocytes isolated from *cx3cr1^{Cre}:r26-YFP* mice according to their gene expression profile. Three main clusters could be identified in these mice with cluster I comprising of 212 cells, cluster II 50 cells and cluster III with 404 cells. Shown are on the X-axis cells and on the Y-axis genes.

(H) Marker gene expression in each cell identifies cluster I as $Ly6C^+$ monocytes, cluster II as $Ly6C^{int}$ monocytes and cluster III as the $Ly6C^-$ subset. Cluster II monocytes were characterized by MHCII gene expression.

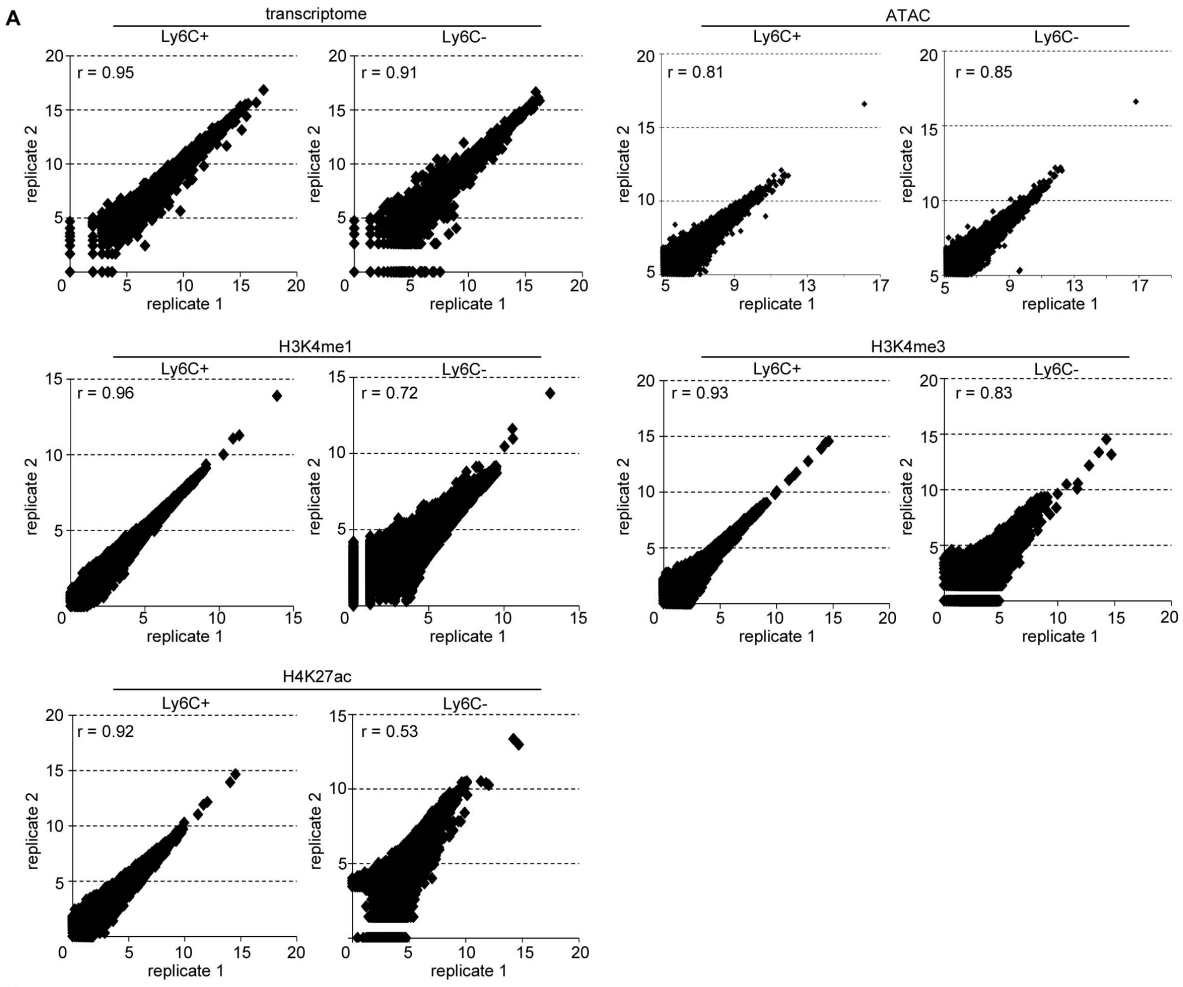

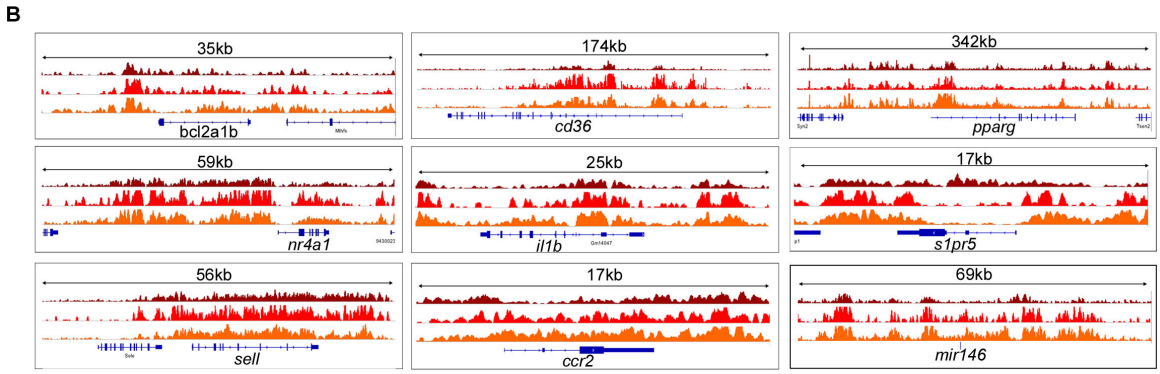

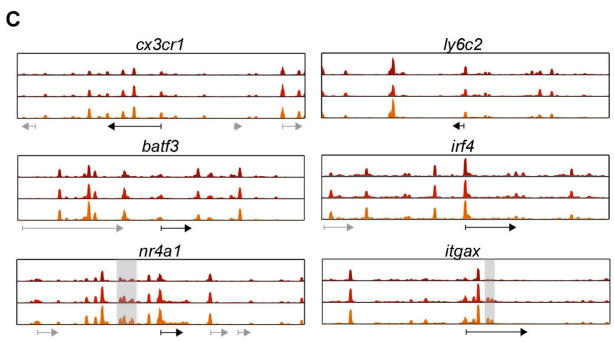

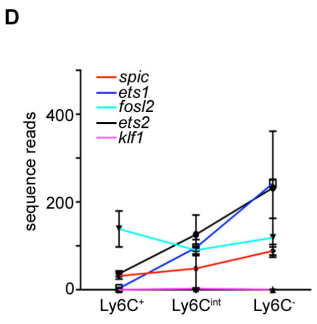

Supplementary Figure 6

Supplementary Figure 6. Correlation of sequencing samples.
Supporting main text figure 4.

(A) Correlation analysis of the duplicates performed for Ly6C$^+$ and Ly6C$^-$ monocytes. Shown are the correlations for RNA-Seq, ATAC, H3K4me1, H3k4me3 and H3k27ac. Data are presented in log_2 values.

(B) Examples of H3K4me1 signal in Ly6C$^+$ (dark red), Ly6C^{int} (red) and Ly6C$^-$ monocytes (orange).

(C) Examples of open chromatin structures in Ly6C$^+$ (dark red), Ly6C^{int} (red) and Ly6C$^-$ monocytes (orange). Shown are IGV tracks spanning 100kb. The location of the indicated gene is depicted as a black arrow. Grey boxes indicate changes in open chromatin areas.

(D) TF expression in Ly6C$^+$, Ly6C^{int} and Ly6C$^-$ monocytes, which were further predicted by Homer motif enrichment as shown in **Fig. 4F**.

Suppl Table 1

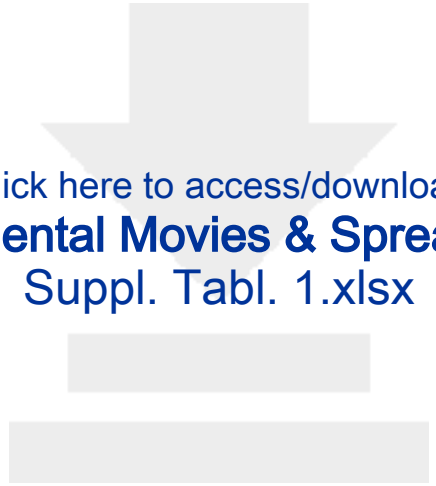

Click here to access/download

Supplemental Movies & Spreadsheets

Suppl. Tabl. 1.xlsx

Suppl Table 2

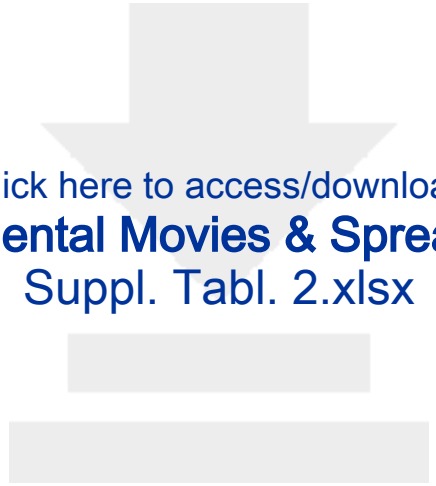

Click here to access/download

Supplemental Movies & Spreadsheets

Suppl. Tabl. 2.xlsx

Inventory of Supplemental Information

Main text Figure 1 is supported by **Supplemental Figure 1 and 2**
Main text figure 2 is supported by **Supplemental Figure 3 and 4**
Main text figure 3 is supported by **Supplemental Figure 5**
Main text figure 4 is supported by **Supplemental Figure 6**

Main text figure 3 is supported by **Supplementary Table 1**

Main text figure 4 is supported by **Supplementary Table 2**